Available online at www.sciencedirect.com
SCIENCE DIRECT®
Remote Sensing of Environment 103 (2006) 379–397
Remote Sensing of Environment
www.elsevier.com/locate/rse

Horizontal radiation transport in 3-D forest canopies at multiple spatial resolutions: Simulated impact on canopy absorption

Jean-Luc Widlowski *, Bernard Pinty, Thomas Lavergne, Michel M. Verstraete, Nadine Gobron

European Commission, DG Joint Research Centre, Institute for Environment and Sustainability, Global Environment Monitoring Unit TP 440, via E. Fermi, I-21020 Ispra (VA), Italy

Received 2 December 2005; received in revised form 1 March 2006; accepted 22 March 2006

Abstract

The divergence of horizontal radiation in vegetation canopies is generally considered to be of negligible consequence to 1) algorithms designed for the physically-based interpretation of space borne observations, and 2) field campaigns aiming at the validation of derived surface products, like FAPAR and albedo. However, non-zero horizontal radiation balances are likely to occur if the internal variability of the vegetation target and the typical distances that photons may travel horizontally within such 3-D media extend to spatial scales that are similar to or larger than those of the measuring sensor. Detailed radiative transfer simulations in 3-D coniferous forest environments are presented to show how the magnitude of local net horizontal fluxes (for spatial resolutions ranging from 1×1 m^2 to 500×500 m^2 forest areas) can reach multiple times the incident solar radiation at the top-of-canopy level. Furthermore, the PDFs of these local net horizontal fluxes (H) are skewed toward negative values (meaning that most local canopy volumes have more radiation exiting than entering via their lateral sides), in particular when the radiative regime is dominated by single-scattering interactions and geometric shading is prominent. In order to maintain the energy balance of the overall forest domain, however, local canopy volumes with rather large positive net horizontal fluxes must also exist, thus underscoring the importance of properly locating local flux measurement equipment. Irrespective of the sign of H, it is shown that the local canopy absorption (A) falls within the $A=H$ (perfect shadowing of the forest floor) and $A=H+1$ (perfect illumination of the forest floor) domain in the red spectral band. This correlation between A and H implies that the range of local canopy absorption values is far larger than unity which reduces its potential to serve as a proxy in delivering accurate domain-averaged absorption estimates on the basis of spatially incomplete sampling schemes. Instead, it is shown that, for a spatial sampling of 1% of the forest area of interest, local absorption estimates – derived from vertical fluxes only – are sufficient for delivering domain-averaged canopy estimates that lie, on average, within 0.05 of the truth. For forest domains that are smaller than about 30×30 m^2, however, horizontal radiation transport will still affect the domain-averaged canopy absorption values and thus a spatially exhaustive sampling of the true local absorption may be more appropriate.

Keywords: 3-D radiation transfer in vegetation canopies; Horizontal photon transport; Validation of pixel-based remote sensing products; In-situ canopy absorption estimates

1. Introduction

At or near the Earth's surface, solar radiation can travel in all directions of the three-dimensional (3-D) space that is available within a volume containing a partially transparent geophysical medium such as vegetation. In canopy studies it is often appropriate to restrict this volume to a box-shaped "voxel" and to categorize the directions of travel of radiation into two broad sets: 1) the downward and upward directions which are needed to identify the contributions due to the vertical transport of radiation across the upper and lower horizontal boundary conditions that define the vertical extent of the voxel, i.e., the Top-Of-Canopy (TOC) level and the vegetation canopy background, respectively and, 2) the horizontal directions involving the contribution from the radiation that crosses the lateral vertical boundaries of this volume of interest. For each of these classes the inward (F^{in}) and outward (F^{out}) oriented fluxes with respect to the corresponding boundaries of the volume of interest can be defined and their balance ($\Delta F=F^{\text{in}}-F^{\text{out}}$), averaged over the entire voxel, can be assessed.

* Corresponding author.
E-mail address: Jean-Luc.Widlowski@jrc.it (J.-L. Widlowski).

0034-4257/$ - see front matter © 2006 Elsevier Inc. All rights reserved.
doi:10.1016/j.rse.2006.03.014

In particular the importance of the radiation traveling upward and downward through the horizontal boundary conditions ($\Delta F_v^{\uparrow\downarrow} = F_v^{\text{in}} - F_v^{\text{out}}$) has long been recognized, e.g., Schuster (1905). Indeed, one of the representations adopted for addressing radiative transfer applications pertaining to volume/domain-averaged quantities is the so-called plane-parallel layer of infinite horizontal extent. This representation implies that, within any local volume bounded by the above upper and lower layer interfaces, the balance between the lateral inflow and outflow of radiation ($\Delta F_h^{\rightleftharpoons} = F_h^{\text{in}} - F_h^{\text{out}}$) is equal to zero or, for all practical purposes, close enough to zero such that its contribution is negligible with respect to the balance involving the vertical radiation transport, i.e., $\Delta F_h^{\rightleftharpoons} \ll \Delta F_v^{\uparrow\downarrow}$. The plane-parallel layer representation constitutes an extreme case in the sense that the lateral boundary conditions cannot even be defined since the surfaces defining the upper and lower boundary conditions are deemed infinitely large. Adopting such a representation is a recognition that the domain-averaged radiation balance, even at local resolution, is strongly controlled by the downward flux of solar radiation, $F_{z^{\text{T}}}^{\text{in}}$ impinging at the upper boundary condition located at the TOC level, z^{T}. Under such conditions, i.e., no net horizontal fluxes, the domain-averaged conservation law involves the radiant fluxes associated with the vertical directions only, i.e., canopy absorption can be described on the basis of the reflected and transmitted fluxes at the upper and lower boundary conditions alone. Closing the energy conservation law on such a system leads to the neglect of the streamflow across the lateral boundary conditions irrespective of the spatial scales considered.

In actual 3-D vegetation canopies, however, it is the location and spatial extent of the upper and lateral boundary conditions that determine the impact of horizontal radiation fluxes in the local energy balance. Here the divergence of lateral radiation streams is unique for every voxel location because 1) the mean free path of radiation in 3-D vegetation canopies is spatially and directionally variant, and 2) the overall horizontal distances that radiation may propagate (and thus also its potential to flow across lateral boundaries of multiple successive volumes of interest) is controlled by both the optical and architectural properties of the canopy together with their internal variabilities. The deterministic nature of plant locations and sizes thus introduces photon channeling and occlusions at the voxel boundaries which make the geometrical aspect of the problem – that is, the spatial extent of the TOC and lateral voxel sides, or, by analogy, the spatial resolution of a sensor or pixel, S and the height of the canopy target, z^{T} – instrumental in determining the relative weight (and sign) of $\Delta F_h^{\rightleftharpoons}$. For instance, the analysis of canopies with TOC heights z^{T} that are much smaller than the voxel (or pixel) spatial resolution, i.e., $z^{\text{T}}/S \ll 1$, does probably not require accounting for the net horizontal fluxes. Indeed, the ratio between the horizontal and lateral dimensions of the boundary conditions is such that radiation can hardly travel far away from its entry point without exiting the canopy layer upward. Conversely, in the case of "tall" canopies, featuring a z^{T} comparable to a significant fraction of S or even larger, radiation may propagate within the canopies (without interacting with the upper horizontal boundary conditions) over horizontal distances which are significantly larger than S. Thus, as the spatial resolution becomes finer the presence (or absence) of lateral shadowing on voxels that are filled with (or empty of) "tall" vegetation will increasingly affect the magnitude and sign of the horizontal radiation balance $\Delta F_h^{\rightleftharpoons}$. At these spatial resolutions a given canopy volume will therefore rarely feature neutral horizontal flux conditions ($\Delta F_h^{\rightleftharpoons} = 0$), but will rather tend to act either as a source (outward > inward and $\Delta F_h^{\rightleftharpoons} < 0$) or a sink (inward > outward and $\Delta F_h^{\rightleftharpoons} > 0$) of radiation for the voxels that surround it. In particular with the current drive toward sensors having finer and finer spatial resolutions, "tall" vegetation canopies–with their strong internal variability of the extinction coefficient (due to foliage clumping and woody structures)–constitute typical scenarios requiring attention during interpretation and validation efforts because of the impact of horizontal radiation transport on the measurable fluxes.

For physical reasons somewhat similar to those exposed here, the contribution due to the net horizontal flux in assessing domain-averaged radiation flux such as albedo and absorption, has long been recognized in the context of cloud physics, e.g., Titov (1990), Cahalan et al. (1994), Titov (1998), Szczap et al. (2000), Marshak and Davis (2005). The quasi-conservative scattering conditions prevailing in clouds, at least at short solar wavelengths, give rise to significant horizontal transport of radiation. At the same time horizontal cloud heterogeneity provides ample opportunities for the occurrence of net horizontal fluxes at local resolutions, i.e., when the sampling scale S is smaller than the typical horizontal distances that photons travel. Neither the geometrical dimensions of vegetation canopy systems nor the scattering properties prevailing in such media can give rise to effects due to net horizontal fluxes that are comparable to those estimated in the cloud physics context. The net horizontal flux of radiation, however, can be expected to play a significant role in at least two categories of land surface applications both linked to the analysis of radiation transfer quantities collected at high/very high spatial resolution, namely 1) validation experiments conducted with ground-based instruments at very high spatial resolutions (e.g., S being a few tens of centimeters to a couple of meters), and 2) quantitative interpretations of data collected by air- or space borne instruments having narrow field of view sensors (e.g., S being of the order of a few meters to tens of meters).

The first one of these categories relates to the validation of global products that are operationally available from space agencies, and that are derived from physically based retrieval algorithms interpreting reflectance measurements of individual pixels from medium resolution sensors such as the MODerate resolution Imaging Spectroradiometer (MODIS), the Multi-angle Imaging SpectroRadiometer (MISR), the MEdium Resolution Imaging Spectrometer (MERIS), and the Sea-viewing Wide Field-of-view Sensor (SeaWiFS) to name but a few, e.g., Knyazikhin et al. (1998), Schaaf et al. (2002), Gobron et al. (1999), Mélin et al. (2001), Diner et al. (2005). These products include notably radiant flux-based quantities such as the surface albedo (see for example http://edcdaac.usgs.gov/ and http://eosweb.larc.nasa.gov/), defined at the TOC level, in multiple spectral regions of the solar domain, as well as the

fraction of absorbed radiation by vegetation canopies at short solar wavelengths (see for example http://fapar.jrc.it/ and http://envisat.esa.int/). These algorithms implement solutions of the radiative transfer problem on a pixel by pixel basis and thus neglect the impact of the net horizontal flux of radiation. The nominal spatial resolutions of the instruments used for generating these products are, in all likelihood, coarse enough to justify the neglect of this contribution in the retrieval of the operational products. When performing product validation, however, the divergence of horizontal radiation is almost certainly going to affect any local measurements/estimates of these flux quantities. Indeed, current validation exercises require, at some point, the development of upscaling procedures involving, for instance, Landsat or SPOT measurements (S is within a few tens of meters) and, consequently, an adjustment or fine tuning of the retrieval algorithm to cope with such increasing spatial resolutions (Tian et al., 2002; Wang et al., 2004). This situation is getting even more complex when conducting product validation directly against ground-based measurements which is the ultimate goal of any validation exercise (Gobron et al., in press).

The second area where the divergence of horizontal radiation will have to be accounted for relates to the accurate retrieval of quantitative information from individual target locations, i.e., pixels, observed at very fine spatial resolutions. Depending on the height of the target, z^{T} and the spatial resolution of the observing sensor S, the magnitude of the radiation streams that enter and exit a given canopy volume via its lateral boundaries can only be ignored if 1) they are insignificant with respect to the vertical fluxes at the target location, i.e., $\Delta F_h^{\rightleftharpoons} \ll \Delta F_v^{\uparrow\downarrow}$, or 2) they are in balance with each other, i.e., $\Delta F_h^{\rightleftharpoons} = 0$ and identical to the corresponding fluxes arising from adjacent canopy volumes of equal dimensions. These latter radiative conditions are met when all architectural and spectral target properties within the field of view of the observing sensor are statistically identical to those in adjacent regions of similar size S, and the typical horizontal distances that photons travel within such a medium are smaller than S. For any given vegetation canopy system the spatial resolution, S^* at which the statistical properties of the canopy become invariant of the position of the sampling domain, i.e., they are said to reach *stationarity* (Davis et al., 1996), thus constitutes a rather critical resolution with respect to the development of pixel-based inversion procedures. In summary, when $S > S^*$ then "pixel-based" inversion schemes can be safely adopted, while contextual or "image-based" algorithms should be developed when $S < S^*$.

This paper evaluates the impact of the horizontal radiation transport on the estimate of the local canopy absorption within simulated (3-D) forest systems. This problem is addressed for various structural, spectral and illumination conditions and across a wide range of spatial resolutions including the case of the very high spatial resolution of in-situ field instruments. Section 2 formulates the local energy balance equation and identifies the critical spatial resolution S^* relevant for a variety of forest canopy conditions. Section 3 then provides a quantitative assessment of the behaviour of net horizontal fluxes as a function of the spatial resolution, the illumination conditions, and the structural and spectral properties of a given canopy target. Section 4 documents 1) the relationship between net horizontal fluxes and the local canopy absorption sampled at very high spatial resolutions within forest domains of 500×500 m^2, and 2) the impact of sampling size and extent on the accuracy of domain-averaged absorption estimates both with and without explicit accounting of the local horizontal radiation transport. Finally, Section 5 summarizes these findings and discusses some of their implications.

2. Presentation of the approach

Our approach is essentially based on model-simulated scenarios of various forest system conditions. The simulation infrastructure is provided by the 3-D Monte Carlo (MC) ray-tracing model of Govaerts and Verstraete (1998) which is used to estimate the desired radiative quantities at several spatial resolutions. As is usually the case, such a model environment imposes some level of approximation/idealisation when representing the various spectral and structural properties of vegetation canopies, especially when carrying out radiative transfer (RT) simulations at very fine spatial resolutions within a larger overall canopy domain $S_{\mathrm{D}} = 900$ m. Our approach relied on a statistical distribution of foliage elements within individual tree crowns. The outer shape of the tree crown was generated, in accordance with the findings of Rautiainen and Stenberg (2005) for the Scots pine (*Pinus sylvestris* L.) species, using a series of frustrums (a cone whose tip has been cut off parallel to its base) of identical vertical thickness but with different upper and lower radii that were stacked vertically on top of each other (see left panel in Fig. 1). By associating different amounts of foliage with different frustrums it is possible to generate tree crowns having realistic shapes and vertically varying (upward-skewed) Leaf Area Index (LAI) profiles. Various forest scenarios were then generated using a log-normal tree height distribution. The crown width, length, height and LAI were all obtained from a collection of allometric relationships (Widlowski et al., 2003) and are listed in Table 1. The spatial distribution of individual trees was generated using randomly selected x, y coordinates within the available domain $S_{\mathrm{D}} \times S_{\mathrm{D}}$ such that new (smaller) trees do not intersect or overlap with existing (taller) ones. This procedure then yields spatial tree distributions that are close to the random patterns that have been documented – both in field and modeling experiments – for mature coniferous forest, e.g., Lepš and Kindlmann (1987), Szwagrzyk (1992), Kint (2005). Finally, a regular grid of virtual voxels is placed at the center of these 900×900 m^2 canopy domains, in order to perform the various RT simulations, as described below.

2.1. Definition of the net horizontal flux

A volume of interest $V(S, z^{\mathrm{T}}; \mathbf{r})$, called voxel, is defined as a box-like entity having two square-shaped top and bottom surfaces $\mathrm{A}^{\mathrm{T}} = \mathrm{A}^{\mathrm{B}} = S \times S$, and four rectangular-shaped lateral sides $\mathrm{A}^{\mathrm{L}} = S \times z^{\mathrm{T}}$, where S is the nominal spatial resolution of the observing sensor (or, alternatively, the width of the resulting pixel) and z^{T} is the maximum height that the canopy may attain

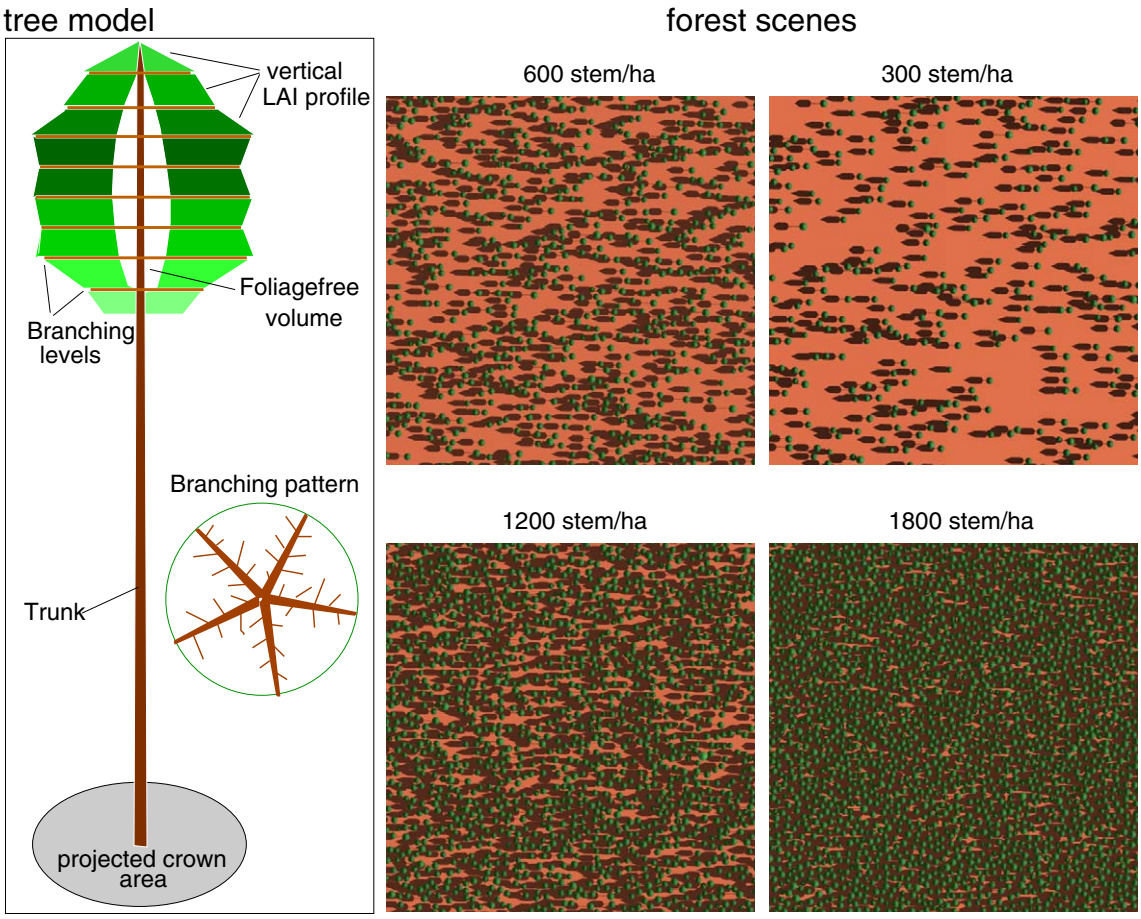

Fig. 1. Left panel: Conceptual graph of a tree model used for the generation of crown architectures with realistic shapes, dimensions and vertical LAI profiles. Various levels of branching can be added in between the various frustrums making up the crown. Right panel: Top view representations of the main four Scots pine forest representations generated for this study ($\theta_0 = 30°$).

within its entire spatial domain S_D. Only the canopy target and not the underlying background is contained within the voxel volume $V(S, z^T; \mathbf{r})$ centered at location $\mathbf{r}$. As described in greater detail in Appendix A, the local energy balance (evaluated at the scale of the voxel volume) can be written as $1 = A(S, z^T; \mathbf{r}) + R(S, z^T; \mathbf{r}) + (1-\alpha)T(S, z^T; \mathbf{r}) - H(S, z^T; \mathbf{r})$, where A is the local canopy absorption, R is the local TOC albedo, and T is the local (direct and diffuse) transmission at the level of the underlying background (that features a spatially uniform albedo α over the entire domain S_D). $H = \Delta F_h^{\rightleftharpoons} / F_{z^T}^{in}$ is the net horizontal flux term (Marshak & Davis, 2005) and results from the integration of the various entering and exiting flux densities across the lateral sides of the voxel and the subsequent normalisation of their difference ($\Delta F_h^{\rightleftharpoons} = F_h^{in} - F_h^{out}$) by the total flux impinging at the top of the voxel, $F_{z^T}^{in}$. The value of H thus indicates the relative weight of the net horizontal power with respect to the incoming power at the TOC reference surface, and can assume either positive or negative values depending on whether there is a net influx or outflow of horizontal radiation into or out of $V(S, z^T; \mathbf{r})$. The more the magnitude of H deviates from zero, the greater is the likelihood that locally measured radiative quantities of a canopy target differ from

Table 1
Structural properties of the 3-D Scots pine forest scenes

Tree density	300	600	1200	1800	[stem/ha]
Tree height (range)	8.75–16.75	8.75–17.75	8.25–17.75	8.25–17.75	[m]
Mean tree height	12.00±1.0	12.00±1.0	12.00±1.0	12.00±1.0	[m]
Tree LAI (range)	2.88–4.16	2.88–4.34	2.81–4.35	2.81–4.35	[m^2/m^2]
Mean tree LAI	3.37±0.16	3.37 ±0.16	3.37±0.16	3.37±0.16	[m^2/m^2]
Height to crown (range)	0.60–13.57	0.60–14.84	0.38–14.84	0.38–14.84	[m]
Mean height to crown	4.53±1.82	4.54±1.82	4.54±1.82	4.54±1.82	[m]
Crown radius (range)	0.71–1.29	0.71–1.39	0.68–1.39	0.68–1.39	[m]
Mean crown radius	0.92±0.07	0.92±0.07	0.92±0.07	0.92±0.07	[m]
LAI of scene	0.270	0.542	1.084	1.628	[m^2/m^2]
Fractional cover	8.0	16.0	31.9	47.9	[%]

measurements of the same quantities acquired at coarser spatial resolutions.

Let's consider the case of a voxel that is completely filled with perfectly absorbing foliage material and that is surrounded by nothing but an infinite expanse of empty voxels overlaying a black background ($\alpha=0$). One may assume furthermore that the lateral sides of this voxel are oriented either perpendicular or parallel to the azimuth of the incident direct solar radiation direction. The net horizontal radiation balance of that voxel, $\Delta F_h^{\rightleftharpoons}$ is then equal to the total flux density entering the voxel through its sunward lateral side, which is proportional to z^{T} S $\tan\theta_0$ — where θ_0 is the Sun zenith angle. At the same time, the total incoming flux density at the upper surface of the voxel is proportional to the area of that surface at the TOC, i.e., $F_{z^{\mathrm{T}}}^{\mathrm{in}} \propto S^2$ (always assuming that the incoming solar light source is spatially uniform). As a consequence the net horizontal flux term $H = \Delta F_h / F_{z^{\mathrm{T}}}^{\mathrm{in}}$ is thus related to z^{T} $\tan\theta_0 / S$ which amounts to a tiny fraction of unity provided that the illumination conditions at the time of overpass are not too oblique ($\tan\theta_0 \leq 1$) and the spatial resolution of the observing sensor is coarse enough ($S \gg z^{\mathrm{T}}$). Under these conditions of observation, i.e., $H(S) \approx 0$, the omission of the net horizontal radiation transport contribution in interpreting remote sensing data is well justified. As the spatial resolution of the observing instrument becomes finer, however, the contribution from $\Delta F_h^{\rightleftharpoons}$ is likely to increase with respect to $F_{z^{\mathrm{T}}}^{\mathrm{in}}$ and consequently H may become significantly different from zero.

In actual 3-D vegetation canopies, however, voxel-shaped canopy volumes do not tend to be filled completely with scatterers and mutual shading often exists between the constituents of neighbouring canopy volumes. As a consequence, less direct solar radiation will enter a voxel laterally, and some of this radiation will pass right through the voxel without affecting its net horizontal radiation balance. Furthermore, actual absorption properties of both the canopy and background constituents differ from unity which will further reduce the magnitude of $\Delta F_h^{\rightleftharpoons}$ by scattering radiation in and out through the lateral sides of the voxel. Overall the role of S, z^{T} and θ_0 in actual 3-D plant canopies is far from obvious when it comes to establishing a spatial resolution threshold S^* beyond which the net horizontal flux term $H(S \geq S^*)$ becomes negligible.

2.2. Assessment of the onset of the stationarity regime

Our goal here is to identify appropriate sampling lengths, S^* that allow for sufficiently accurate estimations of domain averaged canopy properties.[1] In the case of randomly distributed plant populations – a spatial pattern that is relatively common, in particular, among small trees, e.g., Franklin et al. (1985), Moeur (1993), Wu and Strahler (1994) – it is possible to estimate S^* using an ensemble of transects rather than via the analysis of 2-D data arrays. This is because the azimuthal invariance of the plant positions implies that all transects will sample the same processes and thus will also lead to similar moments if their length exceeds S^*. In this context, Davis et al. (1996) proposes, amongst others, the analysis of the running moments, autocorrelation and structure functions in order to identify the minimum spatial scale beyond which the properties of a geophysical field become independent of the location of the sampling transect. Running moments are particularly appealing due to their simplicity, and the normalized running mean (of a dataset $\phi(x)$ covering a distance $0 \leq x \leq L$) can be defined for all length scales $0 < S \leq L$ as:

$$m_\phi(S,x) = \frac{1}{S}\int_x^{x+S} \frac{\phi(x')}{m_\phi(L,x)}\,\mathrm{d}x' \qquad 0 \leq x \leq L-S$$

Choosing $x=0$ and averaging $m_\phi(S, 0)$ over multiple data transects (along different directions and locations within the domain of interest) will yield the ensemble averaged normalised running mean $\langle m_\phi(S)\rangle$ for all transect lengths $S \leq L$.

The various panels of Fig. 2 display $\langle m_\phi(S)\rangle$ as a function of averaging length S for selected radiative (main panel) and structural (inlaid panels) canopy properties up to scales of $S=500$ m. More specifically the local albedo at the TOC, as well as, the LAI, stem density and mean tree height of the canopy were determined at a spatial resolution of 1 m throughout the 900×900 m^2 domain of both a sparse (300 stem/ha) and a dense (1800 stem/ha) Scots pine forest representation. The computation of $m_\phi(S, 0)$ was subsequently applied along various transects of these 2-D geophysical fields, and shows – after ensemble-averaging – a gradual stabilisation with increasing averaging length S. In the main graph of Fig. 2 it can be seen, for example, that the ensemble averaged normalised running mean for the directional–hemispherical reflectance (DHR) of the 300 and 1800 stem/ha Scots pine forests approaches unity at spatial resolutions between 50–60 m in the NIR and 90–110 m in the red wavelengths ($\theta_o=30°$). Obviously the exact location of S^* depends somewhat on the choice of the tolerable deviation that $|1-\langle m_\phi(S)\rangle|$ is not allowed to exceed. Intuitively one would expect that multiple scattering interactions would make the radiative field less susceptible to structural variations and thus lead to smaller values of S^*, i.e., in particular in the NIR and for high vegetation densities. By comparison the analysis of structural canopy parameters with $\langle m_\phi(S)\rangle$ yields plots that are far less "smooth" in their appearance than those of radiative quantities, like the DHR. In the case of the 1800 stem/ha scene (right inlaid graph) the onset of stationarity ($S^* \sim 80$–100 m) occurs at similar spatial resolutions for all three structural parameters depicted, i.e., the LAI, the tree density and the tree height. For the 300 stem/ha forest scene, however, the plots are rather "noisy" and S^* may be different for the various structural parameters depicted.

Further statistical analysis (not shown) of 200 structurally different Scots pine forests (Widlowski et al., 2004) having $4\ \mathrm{m} < z^{\mathrm{T}} \leq 25$ m, tree densities between 8 and 7150 stem/ha, and LAI values ranging from 0.25 to ~ 7 m^2/m^2 indicated that the magnitude of S^* could range from several tens of meters up to 200–250 m. For any one of these 3-D forest representations–featuring randomly distributed trees on a horizontally infinite background–the actual magnitude of S^* depended, however, on the choice of the metric, the size of the available dataset and the variable used in the analysis. For example, when retrieving S^*

[1] Even though, technically, stationarity means invariance of all statistical properties of a geophysical field irrespective of the location of the sampling.

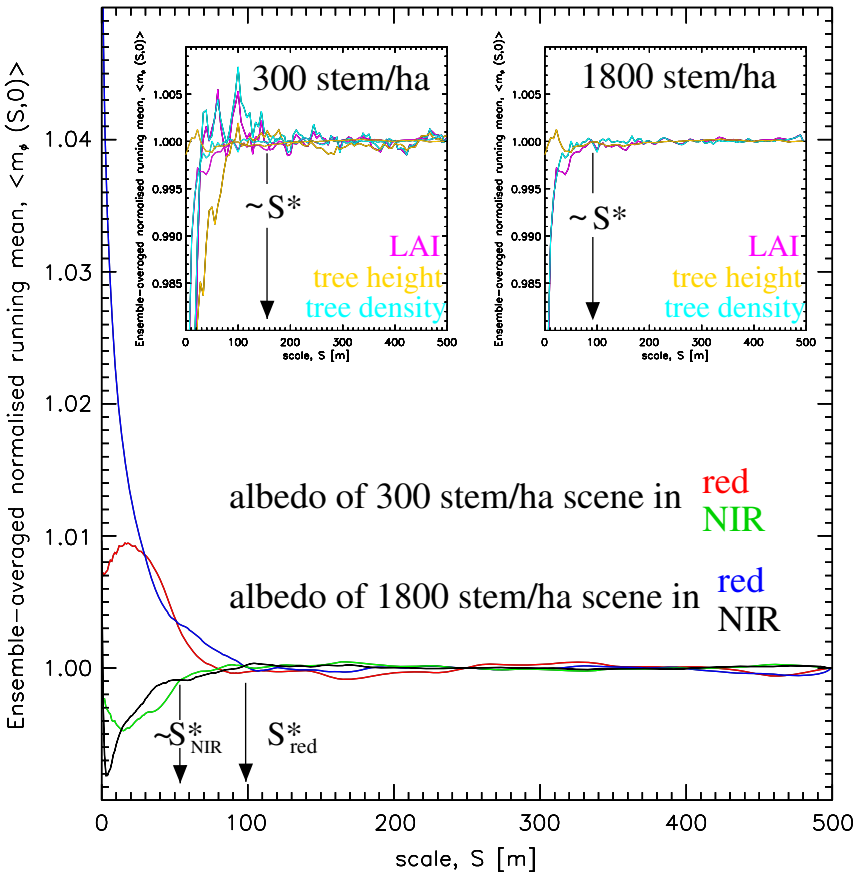

Fig. 2. Ensemble-averaged normalised running mean estimates of radiative (main panel) and structural (inlaid graphs) canopy properties to estimate the spatial resolution, S^* characterising the onset of stationarity for these variables. Main panel: results for the albedo (directional hemispherical reflectance) in both the red and near-infrared (NIR) for a 300 and 1800 stem/ha forest scene ($\theta_0=30°$). Inlaid panels: results for the leaf area index (LAI), tree height and tree density parameters for the 300 (left graph) and 1800 (right graph) stem/ha canopies. (For interpretation of the references to colour in this figure legend, the reader is referred to the web version of this article.)

from structural parameters (like the local LAI, fractional cover, or canopy height) its magnitude tended to be larger than when derived from radiative quantities (like the local albedo, or direct transmission), in particular when the latter are smoothed by substantial multiple scattering contributions. In any case, regardless of these variations in the estimate of S^* for individual forest architectures, the range of S^* values that were retrieved for the entire set of 3-D Scots pine canopies agreed very well with the 100–300 m transect lengths recommended by Chen and Cihlar (1995) and Chen et al. (1997) using the Tracing Radiation and Architecture of Canopies (TRAC) instrument. Our radiation transfer simulations in the red spectral region showed that – at a spatial resolution of $S=250$ m – the maximum net horizontal flux term encountered among the above 200 coniferous forest scenes amounted to only 0.3% of the incident radiation at TOC, which is a negligible fraction for most if not all application purposes. As discussed extensively in Gobron et al. (in press), a significant number of land surface types such as for example grasslands, dense rainforests, and tundra exhibit less internal variability of the extinction coefficient and, consequently, smaller values of S^* and $H(S=250\text{ m})$ than those reported here which are typical for coniferous forests. As such, most terrestrial surfaces can be expected to manifest structural and radiative stationarity when sampled with medium spatial resolution sensors like MERIS, MODIS, SeaWiFS and MISR (having S ranging from $\approx$250 m to 1.5 km). Under these conditions of observations, i.e., for $H(S>S^*;\ \mathbf{r})\approx 0$, the resulting energy balance is simply given by: $A(S;\ \mathbf{r})+R(S;\ \mathbf{r})+(1-\alpha)T(S;\ \mathbf{r})\approx A(S_D)+R(S_D)+(1-\alpha)T(S_D)=1$ and, consequently, the concept of "radiatively independent volume" can be adopted for designing pixel-based retrieval algorithms of canopy state variables (Pinty et al., 2004).

3. Assessment of the net horizontal fluxes within forest canopies

It follows from the discussion so far that the spatial resolution of observation, the illumination conditions, and the structural and spectral properties of the canopy target are instrumental in determining both the range and the spatial variability of the net horizontal radiation fluxes. Section 3.1 will describe the behaviour of $H(S)$ when a given domain of interest S_D is observed at different spatial resolutions, S. Section 3.2 then documents the spatial variability of the local net horizontal fluxes under different conditions of illumination, whereas Section 3.3 describes the overall variability of the local net horizontal fluxes within S_D for various structural and spectral canopy scenarios, among others.

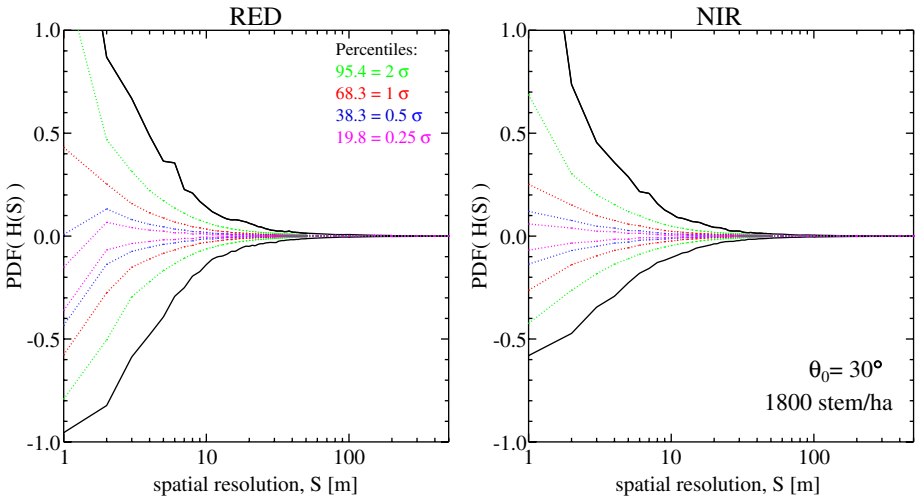

Fig. 3. The PDF of the net horizontal flux term $H(S)$ – when sampled across a larger domain of interest – as a function of the spatial resolution S of sampling. Results are shown for simulations in the red (left panel) and NIR (right panel) spectral domain using an 1800 stem/ha Scots pine forest and $\theta_0=30°$. Indicated are the extreme values (black lines), as well as the 95.4 (green), 68.3 (red), 38.3 (blue) and 19.8 (magenta) percentiles (dotted lines) to each side of the peak of the PDF obtained from a population of several thousand samples in the red or NIR spectral domains. These percentiles correspond to 2, 1, 0.5 and 0.25 standard deviations (σ) in the case of a Gaussian PDF. (For interpretation of the references to colour in this figure legend, the reader is referred to the web version of this article.)

3.1. The variability of net horizontal fluxes across multiple spatial resolutions

Fig. 3 illustrates the evolution of the probability density function (PDF) of the net horizontal flux term, $H(S)$ as a function of the spatial resolution of sampling: $1\ \mathrm{m} \le S \le 500\ \mathrm{m}$. Results are shown for simulations performed in the red (left panel) and NIR (right panel) spectral domain using a regular voxel grid that encompasses a randomly distributed Scots pine forest within an overall domain $S_D=900$ m such that, in all likelihood, $S_D \gg S^*$. The forest has a tree density of 1800 stem/ha, a mean tree height of 12 ± 1 m, and an average crown LAI of $3.37\pm0.16\ \mathrm{m^2/m^2}$ as described in Table 1. The illumination zenith angle was set to $\theta_0=30°$, the Lambertian background had an albedo $\alpha=0.127$ (0.159) in the red (NIR), and the TOC height was taken to be slightly larger than the tallest tree in the forest domain, i.e., $z^T(S_D=900\ \mathrm{m})=17.75$ m. At every spatial resolution S the PDF of $H(S)$ is characterized in terms of its extreme values (black lines), as well as, the 95.4 (green), 68.3 (red), 38.3 (blue) and 19.8 (magenta) percentiles (dotted lines) to each side of the peak of the PDF (obtained from a population of several thousand samples). If the PDFs were Gaussian then these percentiles would be equivalent to 2, 1, 0.5 and 0.25 standard deviations (σ), respectively. Fig. 3 thus shows, first, that the contribution from net horizontal fluxes can be safely ignored when performing retrievals of domain-averaged canopy absorption with sensors operating at resolutions coarser than about 100 m. Second, the extreme values of the PDF of $H(S)$ become asymmetric as the spatial resolution becomes finer. In particular the positive net horizontal flux extreme is getting substantially larger than the negative extreme. This asymmetry is related to the changing ratios of the TOC and lateral voxel sides as described in Appendix B. However, since the domain-averaged net horizontal flux amounts to zero, i.e., the mean of the PDF of $H(S)$ is equal to zero for all sampling dimensions S, the distribution of $H(S)$ must be skewed towards negative values at the finer spatial resolutions. This can be noticed in particular in the red spectral domain, where the peak of the PDF of $H(S)$ – lying between the magenta coloured 19.8 percentiles – occurs somewhere near -0.3 when the spatial resolution becomes comparable to the spatial width of the objects and gaps within the scene ($S=1$ m). In the NIR the predominance of multiple scattering leads to a reduced variability of the PDF of H (at all spatial resolutions) and, by consequence, also to smaller deviations of its peak value from neutrality as the spatial resolution becomes comparable to the width of the objects (and gaps) within the canopy. The large variability of $H(S)$ when $S \ll S^*$, in both panels of Fig. 3, leads to the conjecture that the actual location of a voxel, its vegetation content and degree of lateral illumination all play a significant role in determining the actual value of the local net horizontal flux term.

3.2. The spatial variability of H(S, z^T) at very high spatial resolution

For high spatial resolutions, $S \ll S^*$, the net horizontal radiation flow in and out of $V(S, z^T; \mathbf{r})$ is indeed highly dependent on the position $\mathbf{r}$ of the voxel. This can be seen from the various panels in Fig. 4, showing spatial plots of the net horizontal flux term $H(S, z^T)$ obtained from a regular grid of voxels – with a spatial resolution of $S=1$ m and a height $z^T=17.75$ m – covering a 1 ha subregion of randomly distributed Scots pine trees having a density of 300 stem/ha. Results were generated for both the red (top row) and NIR (bottom row) spectral domains, and for a variety of direct only and diffuse only (left to right columns) illumination conditions. The various shades of red (blue) colours indicate increasing levels of net lateral flux gains (losses) for any given voxel, whereas a white colour is used to point to voxels with well balanced proportions (±5%) of incoming and outflowing radiation streams.

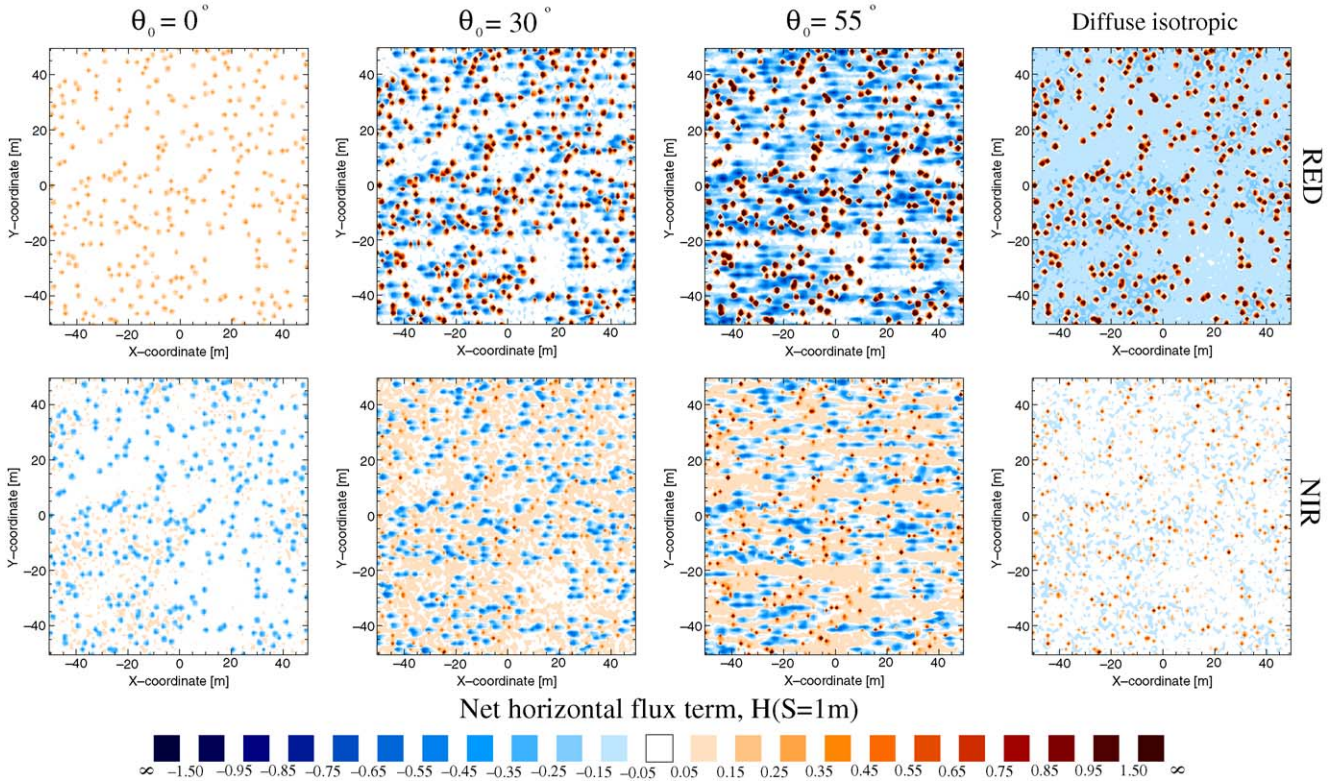

Fig. 4. The net horizontal flux term $H(S=1\text{ m}, z^{T})$ for a 1 ha region of a 300 stem/ha Scots pine forest with $z^{T}=17.75$ m (compare with the top right panel in Fig. 1) under various illumination conditions (columns) in the red (top row) and NIR (bottom row) spectral region. The various shades of red (blue) indicate increasing net energy gains (losses) for any given voxel, whereas a white colour is used to point to voxels with well balanced proportions of incoming and outflowing photon streams. (For interpretation of the references to colour in this figure legend, the reader is referred to the web version of this article.)

- When the Sun is overhead ($\theta_0=0°$) and geometric shading is absent, the spectral properties of the various canopy constituents determine the polarity of the net horizontal flux. In the red spectral domain, where foliage absorption is very high and scattering from the underlying Lambertian background is the primary source of lateral radiation flow, individual tree crowns effectively block the passage of the latter radiation and thereby lead to a net gain of horizontal radiation (light red colour) within voxels that contain foliage. Conversely, in the NIR domain, foliage scattering is very high and constitutes the main source of lateral radiation flow, such that the presence of a tree crown will lead to an enhanced radiation outflow via the lateral sides of the voxel that surrounds it (light blue colour). The absolute magnitudes of $H(S, z^{T})$ are, however, rather small in both spectral regimes and their polarity may even become inverted if the background albedo is sufficiently low (high) so as to make the scattering contribution from the foliage (background) the primary source of lateral radiation flow in the red (NIR).
- When the Sun is at oblique zenith angles ($\theta_0>0°$) geometric shading dominates and accentuates both the magnitudes and spatial variability of the net horizontal flux. Incident direct solar radiation now is the primary source of lateral radiation flow. Absorption events (especially in the red) and scattering out of the voxel via its upper side (especially in the NIR) lead to a positive balance of net horizontal transport of radiation which increases as more radiation is intercepted by the trees within the voxel. Negative net horizontal flux values may occur if the lateral influx of solar radiation is drastically reduced (for example, due to shadowing of a voxel side by neighbouring trees) and the lateral outflow of radiation (due to scattering by the background and foliage) is left to dominate the balance. As the solar zenith angle increases and the shadows lengthen, the number of voxels with a negative balance also increases. At the same time the voxels that contain elongated tree crowns intercept more radiation and by consequence exhibit an increase in the magnitude of their positive H values, in particular in the red spectral domain. In the NIR, small positive H values appear in voxels that do not contain trees and are not affected by geometric shading. This is due to (both direct and already scattered) laterally entering radiation that is either being absorbed by the underlying background, or, else scattered upward to leave the target voxel via its TOC side.
- For isotropic diffuse illumination conditions, foliage absorption (scattering) in the red (NIR) results in strong (weak) geometric shading across all directions of photon travel. The greater the number of trees surrounding a foliage-free voxel, the more the latter is shielded from (exposed to) impinging lateral radiation, and the more the relative weight of the lateral outflow of incident diffuse radiation entering via its TOC boundary will be enhanced (weakened). Consequently, for a sparse forest scene as depicted in Fig. 4, most empty

voxels feature slightly negative values of H in the red, whereas voxels that do contain tree crowns are characterised by large positive values of H at that wavelength. In the NIR, on the other hand, multiple scattering weakens both the positive and negative contributions, so that most of the foliage-free voxels feature a quasi-neutral horizontal radiation transport balance, i.e, ±5%.

Since the domain-averaged net horizontal flux $H(S_D)$ is quasi null, the overall contribution due to voxels with positive values of $H(S=1$ m) must be balanced by an equally strong contribution arising from the ensemble of voxels having negative values of H. As can be seen from the various panels of Fig. 4, the manner in which these horizontal flux contributions are distributed spatially and also in terms of their magnitude ranges depends, however, not only on the illumination conditions and structural properties of the canopy but also on its spectral properties. The impact of these factors on the variability of H, as well as on the magnitude of its most likely value within the domain of interest, H^*, will now be further investigated.

3.3. Estimation of the probability distribution functions of H ($S=1$ m, z^T)

Various PDFs of the net horizontal flux term H at a spatial resolution of $S=1$ m were generated from local simulations performed for individual elements of a regular gridded virtual voxel array that was overlaid onto the randomly distributed 3-D forest constituents in the scene ($S_D=900$ m). The top left panel of Fig. 5 shows the resulting PDFs of $H(S=1$ m) (H expressed in percent), in both the red and NIR domains, for a Scots pine forest of 1800 stem/ha with $z^T=17.75$ m, bounded by a medium bright Lambertian background, and direct illumination conditions with $\theta_0=30°$. In both spectral scenarios the majority of voxels within the canopy domain S_D do not feature neutral horizontal flux conditions. In the NIR, the PDF (black colour) is only slightly skewed with its most likely value H^* occurring in the vicinity of the domain average, i.e., $H^* \approx H(S_D)=0$. This is analogous to the findings of Titov (1998), who considered plane-parallel clouds with fractal liquid water variations along the horizontal directions. In vegetation canopies the impact of geometric shading on H is thus significantly reduced in the NIR domain

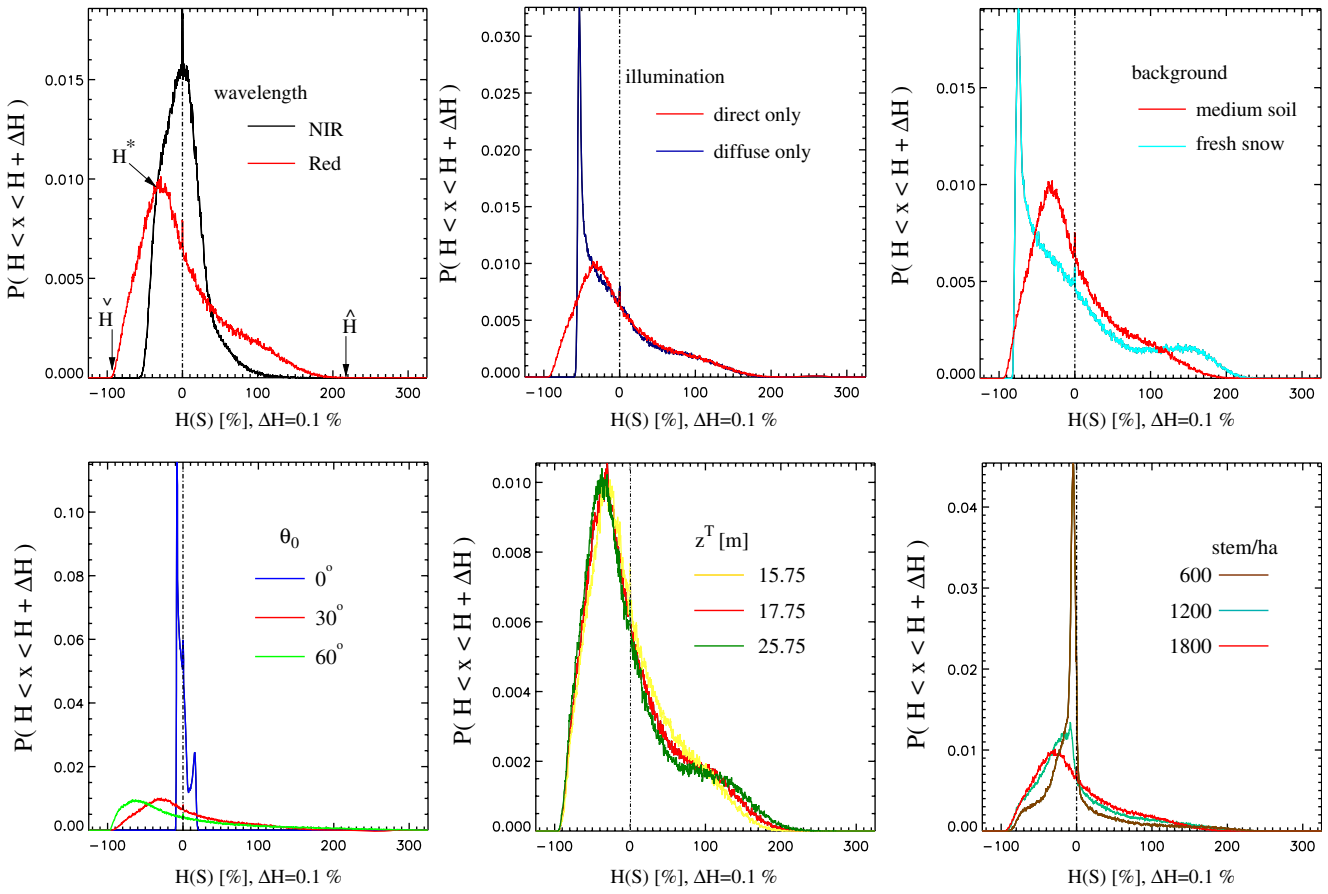

Fig. 5. The probability density function of the horizontal flux term, $H(S)$, obtained from 250,000 different voxel locations at a spatial resolution of $S=1$ m. Each panel displays variations with respect to a default scenario (red colour) which refers to direct illumination conditions ($\theta_0=30°$) in the red spectral domain, for a forest canopy with 1800 stem/ha, $z^T=17.75$ m, and medium soil brightness. The top panels show the PDFs for changing spectral regime (left), illumination types (middle), and background conditions (right). The bottom panels display PDFs for varying solar zenith angles (left), top-of-canopy heights (middle) and tree density conditions (right). (For interpretation of the references to colour in this figure legend, the reader is referred to the web version of this article.)

since shadows tend to be softer in a radiative regime where multiple scattering dominates. In other words the absolute magnitudes of the (positive and negative) net horizontal flux extremes will be smaller under conservative scattering than in a spectral regime where single scattering interactions dominate. This effect is also known as "radiative smoothing", e.g., Marshak et al. (1995), and implies that the variance, or width of the probability density function of H is smaller in the NIR than in the red. In the latter spectral domain, where single scattering enhances the impact of geometric shading, the resulting PDF (red colour) of $H(S=1\text{ m})$ is significantly skewed towards negative net horizontal flux values. This implies that a "typical" voxel features a net leakage of radiation ($H^*<0$) at these spatial resolutions. In other words, the local energy balance of such a voxel, i.e., $[A(S,\ \mathbf{r})+R(S,\ \mathbf{r})+(1-\alpha)T(S,\ \mathbf{r})]\approx 1+H^*$, has a tendency to be somewhat smaller than unity.

Although most voxels in the red spectral domain exhibit negative values of $H(S=1\text{ m})$, the fact that the domain averaged net horizontal flux balance must remain zero, i.e., $\sum_i^N H(S;\mathbf{r}_i)=H(S_D)=0$ with $N=(S_D/S)^2$, implies that some voxels in the scene must exhibit rather large positive values of the net horizontal flux. Indeed, the asymmetry between the absolute magnitude of the maximum positive ($\hat{H}$) and minimum negative ($\check{H}$) value of $H(S=1\text{ m})$ can be directly related to the different areas of the top and lateral sides of a voxel (see Appendix B). The remaining panels of Fig. 5 illustrate the PDF of $H(S=1\text{ m})$ under various structural, spectral and illumination conditions in the red spectral domain. The terms "filled" and "empty" will be used to refer to voxels containing large and small amounts of crown foliage, respectively:

- Diffuse sky illumination conditions (top middle panel) lead to a softening of shadows such that no highly negative H values can occur because there will usually be some radiation entering the voxel via its lateral sides. The multi-directionality of the incident solar radiation thus leads to a "folding" of the most negative section of the original (red coloured) PDF towards more moderately negative values of H. Structural scenarios that 1) allow the diffuse radiation incident at the TOC to traverse the voxel interior largely unobstructed before exiting via one of its lateral sides, and 2) prevent a similar flow of lateral radiation to enter the voxel via its neighbours also contribute to the strong negative peak of the PDF. Such configurations may occur, for example, in voxels that 1) are predominantly "empty" and/or concentrate their vegetation (of low to medium height) in the center of the voxel, and 2) are surrounded by predominantly "filled" voxels containing relatively tall vegetation.
- Bright background conditions (top right panel) allow for more radiation to be scattered laterally out of predominantly "empty" voxels than dark background conditions, thus enhancing the peak of the PDF and shifting H^* towards more negative values. Scattering by bright backgrounds also enhances the interception and absorption of radiation by the canopy foliage, thus shifting moderately positive H regions toward larger magnitudes and thereby increasing the value of the positive PDF extreme, $\hat{H}$. As a consequence fewer voxels will feature quasi-neutral net horizontal flux conditions.
- Large solar zenith angle (θ_0) values (bottom left panel) skew the PDF toward their negative extreme because geometric shadowing becomes more prominent and the scattering contribution from the background is smaller due to lower values of the direct transmission. The positive tail of the PDF is reduced in magnitude because the likelihood for predominantly "filled" voxels to be completely illuminated laterally decreases for dense canopy scenarios as $\theta_0 \gg 0°$. For $\theta_0=0°$ geometric shading does not intervene and the background brightness determines the shape of the PDF. As a consequence, predominantly "empty" voxels will contribute to a negative PDF peak, whereas the "filled" voxels that are surrounded by a sufficient number of "empty" voxels will contribute toward a positive PDF peak. The relative magnitudes of these two PDF peaks depend on the percentage of "filled" and "empty" voxels within the domain of interest.
- Increasing the canopy height (z^T) (bottom middle panel) without changing the canopy structure leads to a larger number of voxels impacted by geometric shading and a consequent increase in the number of voxels with negative H, provided that the stem density is sufficiently low. In the case of dense vegetation targets, the impact of variable canopy heights is limited because the shadows almost never reach the underlying background but continue to cast the same shadow patterns on the top of the neighbouring tree crowns in the canopy. Contributions from the underlying background, on the other hand, generate a small positive "bump" in the PDFs, because the solid angle of the gaps between the tree crowns gets smaller as z^T increases.
- Large tree density values (bottom right panel) increase the degree of shadowing in between the tree crowns in the scene, thus broadening the peak of the PDF and shifting it toward more negative values. Very sparse canopies have very pronounced PDF peaks close to $H=0$ because most voxels do not feature trees, nor are they affected by geometric shading. On the other hand, those voxels that do contain tree crowns will benefit from optimal lateral illumination such that the positive PDF extreme $\hat{H}$ increases somewhat.

Although certainly dependent on the random (i.e., non-regular) distribution of trees, the above scenarios show that at very high spatial resolutions ($S=1$ m) the PDFs of H are typically skewed toward negative values (with an occasional secondary peak at positive H values). In particular very bright backgrounds (e.g., snow) and isotropically diffuse illumination conditions lead to a sharp rise in the magnitude of the peak of the PDF with the corresponding H^* value being close to -0.75 and -0.55, respectively, at $\theta_0=30°$. The question thus arises as to what the impact of these non-zero net horizontal radiation exchanges may be with respect to local and domain-averaged canopy absorption estimates.

4. The impact of net horizontal fluxes on canopy absorption

The local energy balance states that non-zero net horizontal fluxes affect the true canopy absorption at very high spatial resolutions. Section 4.1 will document the patterns of organisation between these two radiative quantities when sampled at very high spatial resolutions throughout some larger domain of interest ($S_D > S^*$). Section 4.2 will present the impact of sample number and size on domain-averaged absorption estimates, $A(S_D)$ distinguishing between sampling strategies that do and do not account for the presence of local net horizontal fluxes.

4.1. The relationship between H(S = 1 m) and the local canopy absorption

The exact repartitioning of H among the various radiative components A, R and $(1-\alpha)T$ cannot be known a priori. At $S=1$ m, neither the local albedo $R(S, \mathbf{r})$ nor the transmission $T(S, \mathbf{r})$ shows any systematic correlation with the local net horizontal flux. The local absorption $A(S, \mathbf{r})$, however, appears highly correlated with $H(S, \mathbf{r})$ as can be seen from the various panels of Fig. 6. Here the local estimates of $H(S=1$ m, $\mathbf{r})$ and $A(S=1$ m, $\mathbf{r})$ were gathered over a domain of 500×500 m^2, in the red spectral band, and plotted as a two-dimensional (2-D) PDF. The various colours indicate the probability density of H, A pairs (on a log scale) to fall within individual bins of width $\Delta H = \Delta A = 0.05$, such that: $\int_{-\infty}^{\infty}\int_{-\infty}^{\infty} P(H, A)\, dH\, dA = 1$.

The main (left hand) panel features results for a Scots pine forest – with $z^T = 17.75$ m, a tree density of 1800 stem/ha and a medium background brightness – that is illuminated with a source located at $\theta_0 = 30°$. It can be seen that the majority of voxels in the domain of interest exhibits rather small local absorption values, i.e., $A(S=1\text{ m}) < 0.1$. This is related to the fact that the spatial extent of the voxels ($S=1$ m) is similar to the width of the individual tree crowns so that only very few voxels will actually contain a whole tree crown. Indeed most of the voxels in the domain of interest will be half-empty and at least partially affected by shadowing which reduces the degree of direct lateral illumination with the consequence that $H<0$. Geometric shadowing will tend to affect multiple adjacent voxels at a time since the height of individual tree crowns can be up to several times their width. By the same token those voxels that do experience unobstructed lateral illumination conditions and that also contain large fractions of vertically elongated tree crowns will tend to intercept (and absorb) more radiation than is available at their TOC level. This is confirmed by the significant number of the local canopy absorptions that exceed unity – in the main panel of Fig. 6 – and that may even reach values of $A(S=1\text{ m}) > 2$, in particular, if accompanied by a similar net horizontal flux value. In the red spectral domain, where single-scattering interactions prevail, this correlation between $A(S=1$ m) and H ($S=1$ m) may be expected since both quantities are defined with respect to the incident flux at the TOC, and are thus increasingly affected by the ratio of the lateral to TOC voxel areas (which is $z^T \tan\theta_0 / S$) if $S < z^T$. Indeed, the various panels of Fig. 6, where $S = z^T / 17.75$, reflect this behaviour. Somewhat more interesting, perhaps, is that (H, A) data pairs that were located close to the right hand side of the 2-D PDF were found to feature almost completely illuminated voxel backgrounds, whereas those on the left hand side of the 2-D

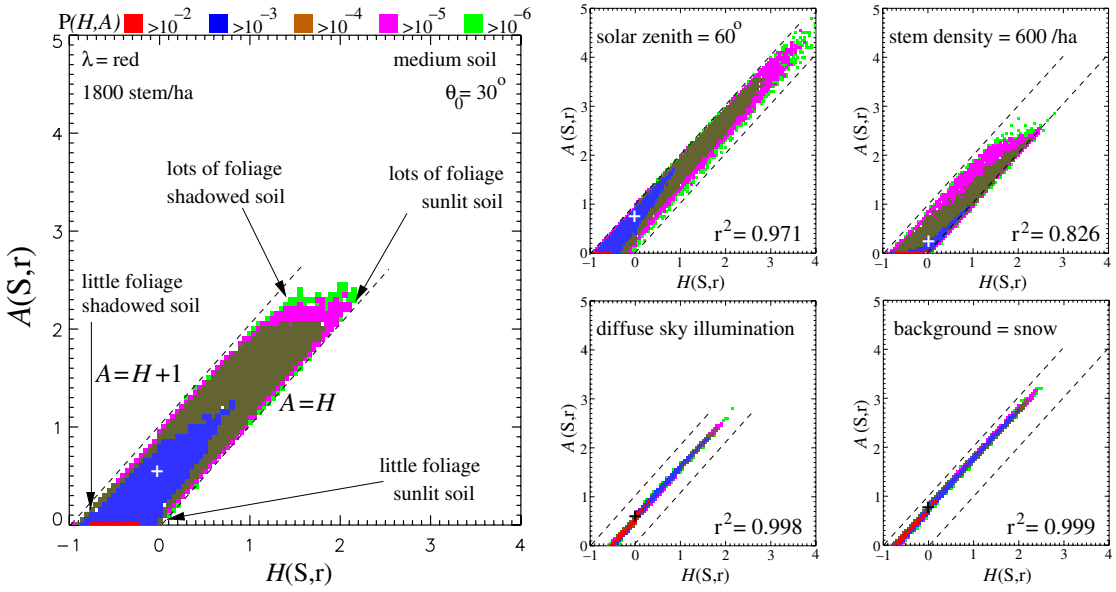

Fig. 6. The 2-D probability density function, $P(H, A)$ of the net horizontal flux term $H(S, z^T; \mathbf{r})$ and the local canopy absorption $A(S, z^T; \mathbf{r})$ obtained from a population of 250,000 voxels with a spatial resolution of $S=1$ m each. The main panel shows results obtained in the red band for a 1800 stem/ha Scots pine forest with medium soil brightness conditions, direct illumination only ($\theta_0 = 30°$). Right panels show 2-D PDFs of H and A for $\theta_0 = 60°$ (top left), tree density = 600 stem/ha (top right), diffuse sky illumination (bottom left) and very bright background (bottom right) conditions (all other parameters remain the same). The domain-averaged absorption $A(S_D)$ is indicated by a white cross, and the magnitude of P(H, A) is given on a logarithmic scale according to the colour legend displayed on top of the main panel. (For interpretation of the references to colour in this figure legend, the reader is referred to the web version of this article.)

PDF received almost no radiation at the bottom of the voxels (shadowed background).

For the sake of better understanding the observed $P(H, A)$ patterns, extreme conditions with $R=0$ and $\alpha=0$ can be assumed, such that the local energy balance (Eq. (4) in Appendix A) can simply be written as $A=1-T+H$. Assuming further that the background of the target voxel is completely shadowed, that is, the local transmission is equal to zero ($T=0$), leads to the leftmost boundary of the $P(H, A)$ in the main panel of Fig. 6, i.e., $A=1+H$. Alternatively, one may assume that the local transmission is equal to unity which may occur, for example, if the perfectly absorbing foliage fills only the upper part of the voxel and the neighbouring voxel on the sunward side is empty. In this case the background of the target voxel is completely illuminated ($T=1$) and the local energy balance reduces to the rightmost boundary of the $P(H, A)$ in the main panel of Fig. 6, i.e., $A=H$. Now, even though the background albedo is always greater than zero and full foliage absorption never occurs in actual forest canopies the spectral properties of such environments remain sufficiently small in the PAR region of the optical spectrum to yield (H, A) data pairs that are constrained by the above two limiting cases. This can be seen from the various panels in Fig. 6 which also feature the domain-averaged absorption, $A(S_D)$ of the canopy (the barycentre of the 2-D PDF) indicated as a white cross along the $H=0$ line. The impact of different (with respect to the conditions described in the main panel) illumination conditions, vegetation structures and optical properties are illustrated in the various panels in the right hand part of Fig. 6:

- Increased solar zenith angle values will enhance the radiation interception and geometric shading of the vertically elongated tree crowns. As a consequence both the local canopy absorption A and the net horizontal flux term H will tend to increase (up to 5 times the level of the incident radiation at the TOC) provided that sufficient gaps exist in the canopy to illuminate the lateral sides of the voxels. At the same time, however, the enhanced geometric shadowing will lead to a reduced direct transmission T through the canopy such that shadowed backgrounds will become more prominent. The net results of these changes thus are a greater range of the (H, A) data pairs, and a skewing of the 2-D PDF towards the $A=H+1$ (shadowed background) line, respectively. By the same token the domain-averaged canopy absorption will shift towards higher values.
- Reduced (increased) tree densities enhance (diminish) the probability of voxels having illuminated background conditions, i.e., $T\rightarrow 1$ ($T\rightarrow 0$). This manifests itself in a skewing of the 2-D PDF toward the $A=H$ ($A=H+1$) line. Fewer (more) trees also imply that the domain-averaged canopy absorption shifts toward smaller (larger) values.
- Diffuse sky illumination tends to soften shadows and leads to intermediate background illumination conditions throughout the canopy, i.e., T is neither approaching 0 nor 1 and the 2-D PDF of H and A lies about halfway between the $A=H$ and $A=H+1$ lines. At the same time, the multi-directionality of the incoming solar radiation increases the correlation between H and A ($r^2=0.998$).
- Increased background brightness will tend to 1) reduce the net horizontal flux term, H of voxels with brightly illuminated backgrounds due to more radiation being reflected laterally back out of such voxels; this will shift (H, A) data pairs away from the $A=H$ line, 2) increase the canopy absorption A of voxels that intercept radiation scattered upward from the background; this will increase both H and A in equal terms if the radiation first has to enter the voxel laterally, and 3) soften the shadows – cast by incident solar radiation on the canopy floor – due to higher order scattering of diffusely reflected radiation from neighbouring background regions; this will shift the (H, A) data pairs away from the $A=H+1$ line although only a little since vegetation is highly absorbing in the red. Lambertian scattering from a bright background leads to a remarkable correlation of H and A ($r^2=0.999$).

The above findings reveal that the choice of voxel locations is rather important for estimating the local absorption value in randomly distributed tree canopies. Most of the negative net horizontal fluxes tend to be associated with voxels that feature little vegetation content and that suffer from lateral shadowing. Conversely, voxels with large amounts of foliage and substantial lateral illumination tend to exhibit positive net horizontal flux values. Thus, the variability of H is reflected in an equally large variability of the true local absorption within the domain of interest which may in some cases rise to ~5 times the level of the incident radiation at the TOC. The large range of both the local H and A values in Fig. 6 together with their highly skewed distribution may, however, require exhaustive sampling of the overall domain S_D to yield accurate estimates of the domain level absorption $A(S_D)$. From Section 2.2 it is known that the net horizontal flux is negligible for $S_D > S^*$ such that $A(S_D)=\frac{1}{N}\sum_i^N A(S=1\text{ m}, \mathbf{r}_i) \approx \frac{1}{N}\sum_i^N A^{\updownarrow}(S=1\text{ m}, \mathbf{r}_i)$ where $N=(S_D/S)^2$ and $A^{\updownarrow}(S, \mathbf{r}_i)=1-R(S, \mathbf{r}_i)-(1-\alpha)T(S, \mathbf{r}_i)$ corresponds to the local energy balance estimated from the vertical flux contributions only. Unlike H and A, the quantity $A^{\updownarrow}$ has the advantage that all fluxes involved in its estimation relate to identical surface areas. As such the variability of $A^{\updownarrow}(S)$ can be expected to be smaller than that of $A(S)$ in particular if $S<z^T$.

Fig. 7 shows a series of PDFs of $A^{\updownarrow}(S=1\text{ m})$ – with $A^{\updownarrow}$ expressed in % – that were obtained from RT simulations in the red spectral band for both sparse (left) and dense (right) canopy structures under various illumination conditions. These PDFs deviate from Gaussian-looking shapes as soon as direct solar illumination conditions are considered (in which case $A^{\updownarrow}(S=1\text{ m})$ may also attain negative values due to unaccounted lateral radiation fluxes—see left panel of Fig. 7). Fortunately, however, most of the currently used optical field instruments, like the LAI-2000 Plant Canopy Analyser (Li-Cor Inc., Lincoln, NB, USA) and the AccuPAR Linear PAR Ceptometer (Decagon Inc., Pullman, WA, USA), are to be operated under diffuse illumination conditions (Morisette et al., in press) which should facilitate the spatial sampling strategy. But even for direct solar

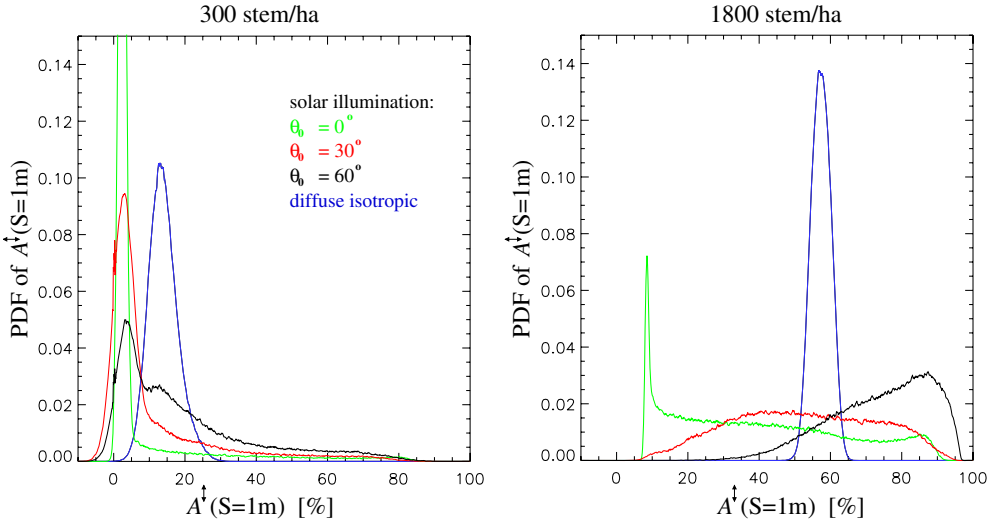

Fig. 7. The PDF of the local absorption $A^{\updownarrow}(S)$, estimated from up- and downwelling hemispherical fluxes at the TOC and background only, sampled in the red spectral band and at a spatial resolution of $S=1$ m from a population of several thousand locations. Results are shown for sparse (left panel) and dense (right panel) forest canopies under a variety of illumination conditions. (For interpretation of the references to colour in this figure legend, the reader is referred to the web version of this article.)

illumination conditions, the variability of $A^{\updownarrow}(S=1\text{ m})$ is always substantially smaller than both that of $A(S=1\text{ m})$ and $H(S=1\text{ m})$ within the domain S_D (compare Fig. 7 with the findings of Figs. 5 and 6). This supports the design of sampling campaigns that rely on in-situ measurements of vertical fluxes only to obtain local estimates of $A^{\updownarrow}$, e.g., Huemmrich et al. (2005), Turner et al. (2004), that may subsequently be aggregated to yield an estimate of the domain-averaged canopy absorption $A(S_D)$. From the discussion of Section 2.2 one may, however, expect that this may be appropriate only for relatively sparse sampling strategies within canopy domains having $S_D > S^*$. For smaller domain sizes, i.e., $S_D < S^*$, the net horizontal fluxes can be expected to remain important at the level of the domain-averaged absorption.

4.2. The impact of net horizontal fluxes on domain-averaged absorption estimates

Exhaustive sampling of the radiation fluxes in vegetation canopies is a laborous, expensive and also time consuming undertaking. Changes in illumination conditions (both in terms of the direct and diffuse components) will affect both the incident flux at the TOC and the shapes of the resulting PDFs for both H and A, which – no doubt – will complicate the accurate estimation of domain-averaged flux quantities. As a consequence, and in "tall" forest environments also as a practical necessity, the up- and downwelling radiation at the TOC is often evaluated from a single location only – using devices mounted on instrumented towers or cranes – while the same quantities at the bottom of the canopy may be sampled relatively fast over somewhat larger spatial areas. Such an approach then raises the question as to how many point measurements are required and how these should be interpreted and/or combined in order to accurately estimate domain-averaged radiation quantities. This section will, however, not address the up-scaling of individual surface albedo measurements – which will depend both on the spatial variability of the canopy target and the height of the tower where such measurements are being carried out – but rather report on the deviations that can be expected between the true domain-averaged canopy absorption and aggregations of local absorption estimates carried out over spatial domains of varying extent.

More specifically, the various panels of Fig. 8 document the mean absolute deviation that exists between the true domain-averaged canopy absorption $A(S_D)$ (in the red spectral regime) and the arithmetic mean of an ensemble of local ($S=1$ m) canopy absorption estimates covering a fraction f [%] of the total area of the canopy domain of interest, i.e., $\langle A(S=1\text{ m})\rangle_f = \frac{1}{n}\sum_i^n A^*(S=1\text{ m}, \mathbf{r}_i)$ where the total number of samples $n=0.01\ (S_D/S)^2\ f$. Results are shown for increasing domain sizes S_D and account for multiple instances of randomly drawn sampling locations within the regular voxel grid that covers the domain of interest, as well as, for multiple instances of domain locations within the forest canopies. Dashed lines indicate that the local absorption estimates were derived using the vertical fluxes only, i.e., $A^*=A^{\updownarrow}$, whereas solid lines show that the local absorption measurements accounted for the horizontal fluxes as well, i.e., $A^*=A$. Colours indicate the spatial extent of local sampling, i.e., $f=1\%$ (azur), 10% (magenta), 25% (blue), 50% (green) or 100% (red) of the total area of the domain of interest S_D (for a domain size of $S_D=100$ m, for example, this would correspond to 100, 1000, 2500, 5000, and 10,000 local measurements, respectively). The panels on the left (right) refer to a sparse (dense) forest canopy, that is being illuminated under isotropically diffuse conditions (top), or, with a direct solar component having either $\theta_0=30°$ (middle) or $\theta_0=60°$ (bottom).

The various panels of Fig. 8 show a decrease in the average bias of the domain-averaged canopy absorption estimate $|A(S_D) - \langle A^*(S=1\text{ m})\rangle_f|$ as the size of the domain increases towards S^*. This is related to the fact that 1) the number of local samples n has to increase in order to retain a spatial sampling of f percent

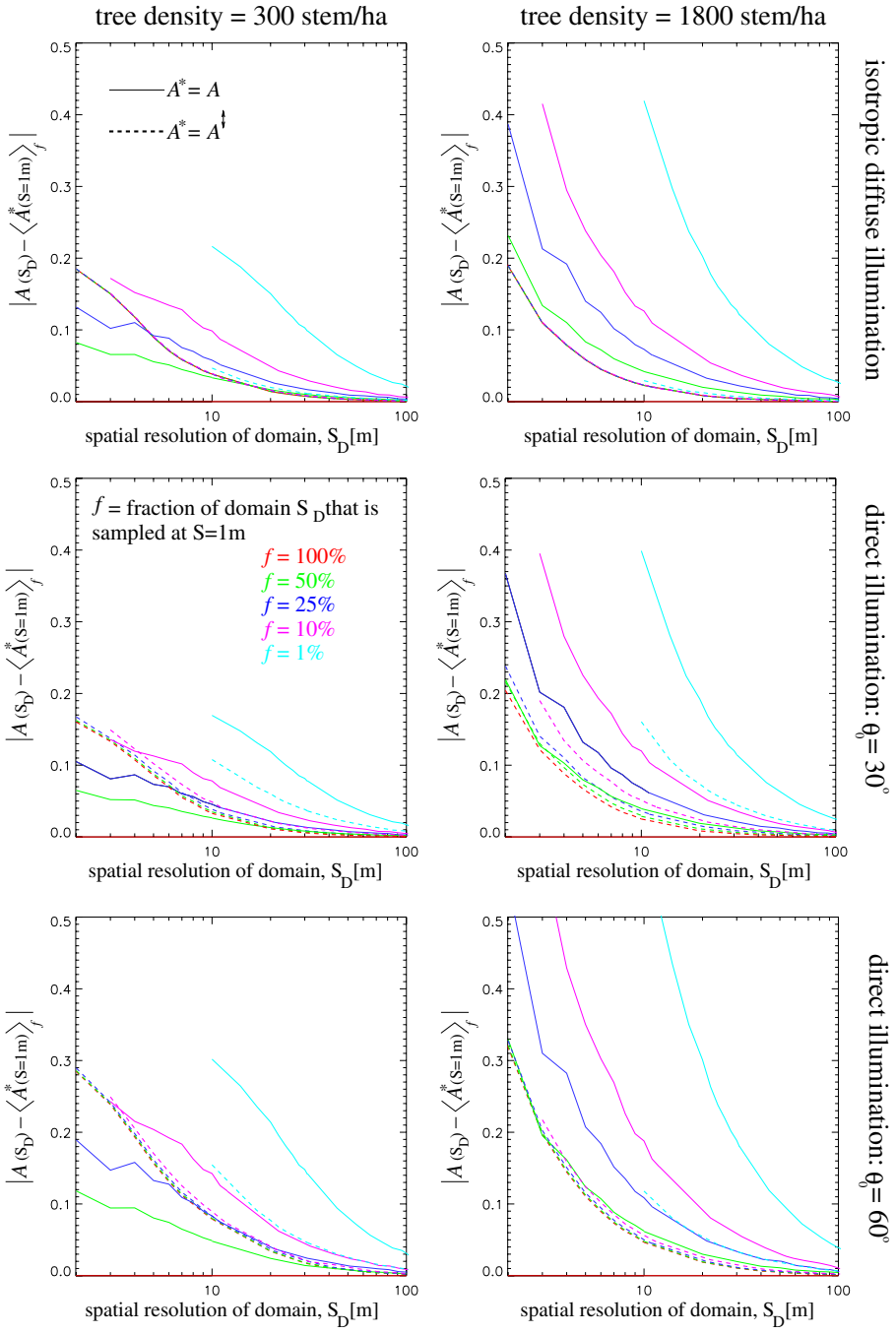

Fig. 8. The mean absolute deviation between the true domain-averaged absorption $A(S_D)$ and the ensemble average of local canopy absorption measurements $\langle A^* \rangle$ (carried out at a spatial resolution $S=1$ m over some fraction f [%] of the domain of interest), plotted as a function of the size of that domain, S_D. Dashed lines indicate that the local absorption estimates were derived from vertical fluxes only, ($A^*=A^{\downarrow}$), whereas solid lines show that the local absorption measurement accounted for the horizontal fluxes as well ($A^*=A$). Colours indicate the extent of local sampling, i.e., $f=1\%$ (azur), 10% (magenta), 25% (blue), 50% (green) or 100% (red) of the total area of the domain of interest S_D. Panels on the left (right) refer to a sparse (dense) forest canopy, that is illuminated either under isotropically diffuse conditions (top), or, with a direct solar component only having $\theta_0=30°$ (middle) or $\theta_0=60°$ (bottom). (For interpretation of the references to colour in this figure legend, the reader is referred to the web version of this article.)

of the area of the domain of interest S_D, and 2) the spatial resolution, S^* that conserved the (structural and spectral) statistics of the canopy was smaller than the overall extent of the canopy domain, S_D. In the case of exhaustive spatial sampling ($f=100\%$) the sampling method accounting for horizontal fluxes is obviously identical to $A(S_D)$ across all domain sizes (red solid line), whereas the sampling method that uses vertical fluxes only exhibits an average absolute deviation of 0.16 to 0.32 at $S_D=2$ m, and <0.01 at $S_D=100$ m, with respect to the true domain-averaged absorption $A(S_D)$. In the case of incomplete spatial sampling strategies the situation is quite different however. Here, domain-averaged absorption estimates, that were derived from vertical flux measurements only (dashed lines), are on average better than those using the true local

absorption (solid lines) in particular in the case of the dense forest canopy where this holds for all domain sizes even when the sampling extent, f increases to 50%. In the case of the sparse forest canopy, the pattern is typically the same but may depend somewhat on the spatial resolution of the domain of interest as well as the conditions of illumination. In general, for small values of f and coarse domain sizes, the sampling of $A^{\downarrow}(S=1\text{ m})$ will yield better domain-averaged absorption estimates, whereas for large values of f and fine domain sizes the domain-averaged absorption estimate is better derived from a sampling of the true local absorption $A(S=1\text{ m})$. If one were to place the maximum absolute bias at 0.05 of the domain-averaged absorption then – based on the results of Fig. 8 – exhaustive sampling strategies are recommended for domain sizes below ~15 m, whereas at domain sizes larger than ~30 m a random spatial sampling scheme with $f=1\%$ would be sufficient. As such the validation of remotely sensed canopy absorption products, derived from medium to coarse spatial resolution sensors over forested targets of uniform spatial heterogeneity, could be performed by sampling less than 1% of the sensor's footprint area, in particular, if the tolerable maximum absolute bias can reach 0.1 or more.

5. Concluding remarks

Highly structured vegetation canopy systems, such as coniferous forests, are characterized by a significant spatial variability of the extinction coefficient which translates itself into a continuously changing lateral transport of solar radiation within the overall spatial domain of these environments. Due to the typical spatial scales involved in the sampling of such quantities, i.e., the height of the canopy and the spatial resolution of the sensor, this transport yields values of the net horizontal flux that may exceed those based on vertical fluxes only if the canopy height exceeds the spatial resolutions of the measuring device. We investigated this issue with numerical simulations of radiation transfer processes in realistic 3-D forest environments in order to quantify the magnitude of the net horizontal flux, as well as, its impact on the local and domain-averaged canopy absorption.

It was shown first that the lateral transport of solar radiation concerns spatial resolutions finer than about 100 m and is thus not of prime concern when retrieving domain-averaged absorbed flux from medium resolution sensors in space. At spatial resolution comparable to the width of individual objects in the canopy, the net horizontal flux estimated over local volumes (or voxels) is, on average, highly skewed toward negative values, meaning that the majority of voxels experience a net loss of horizontal radiation, or alternatively, act as sources of horizontal radiation with respect to their surroundings. At high spatial resolutions, geometric shading dominates the net horizontal flux values in coniferous forest canopies, in particular, in the red spectral domain where single scattering interactions prevail. Here, predominantly empty voxels with shaded backgrounds tend to exhibit net losses of horizontal fluxes, whereas well illuminated voxels with lots of foliage feature net gains of horizontal fluxes. In general, the maximum gain of net horizontal fluxes that a voxel may exhibit, exceeds the maximum loss within the domain of interest if geometric shading prevails and the spatial resolution of the sensor is less than the top-of-canopy height. At very high spatial resolutions ($S=1$ m) the PDFs of the net horizontal flux values are thus non-Gaussian even when sampled over canopy domains S_D that are large enough to guarantee the stationarity of the various structural and spectral canopy properties. In fact, the skewness of these PDFs is further enhanced by large solar zenith angles, bright background albedos and diffuse illumination conditions if the radiative transfer in the medium is dominated by single scattering interactions. Consequently the net horizontal flux extremes tend to be larger in the red spectral domain than in the near-infrared where the prevalence of multiple scattering leads to a radiative smoothing of the various flux quantities.

A remarkable correlation between the net horizontal flux H and the local absorption A was found in the red spectral domain, in particular under the occurrence of diffuse illumination or in the presence of a very bright background. The range of values for both of these flux quantities may, however, span multiple times the level of the incident solar flux at the TOC. At the same time, their highly skewed PDFs may prevent any accurate estimate of the domain-averaged canopy absorption without a spatially exhaustive sampling scheme. In fact, the spatial variability of both H and A is always larger than that of $A^{\downarrow}$, i.e., the local canopy absorption based on the measurement of vertical fluxes only, in particular, if the spatial resolution of observations is smaller than the canopy height. The selective spatial sampling of $A^{\downarrow}$ is thus the most appropriate measurement strategy in field campaigns aiming to retrieve accurate domain-averaged absorption estimates. Our results show that under isotropically diffuse illumination conditions a spatial sampling of $A^{\downarrow}(S=1\text{ m})$ that covers 1% of the surface area of the domain is sufficient to estimate the domain-averaged absorption to within 0.05 on average (dashed lines in Fig. 8), provided that the domain size is not smaller than ~10 m (~30 m for direct solar illumination conditions with $\theta_0=60°$). For domain sizes that are smaller than this, better results can be achieved using a complete spatial sampling of the domain, and – in particular for $S_D<10$ m – measurements of the local canopy absorption that do account for the divergence of horizontal radiation. This is because the lateral radiation transport is capable of affecting domain-averaged radiative quantities at these domain sizes.

These findings have obvious implications for the validation of quantitative information derived from multi-angular and/or multi-spectral remote sensing measurements over individual target locations (pixels). For sensors with very high spatial resolutions – and, in particular, in the case of tall vegetation canopies with substantial internal variability – an accurate knowledge of the location and extent of single pixels on the ground (together with the shape of the point spread function of the sensor) will be necessary to account correctly for the lateral radiation streams that enter and exit the canopy target. Furthermore, due to the significant impact of geometric shading on the horizontal radiation fluxes in the PAR region (400–700 nm) it may actually become necessary to perform in-situ

measurements under illumination conditions that are as close as possible to those occurring during the satellite overpass. On the other hand, when it comes to the validation of remote sensing products derived from medium to coarse spatial resolution sensors, horizontal fluxes can safely be ignored during validation campaigns and the issue reduces to identifying optimal ways to combine point measurements into accurate estimates of domain-averaged canopy properties. In particular, if the uncertainty of the domain averaged canopy absorption or surface albedo estimate has to lie within similar levels as the radiances measured by current space sensor (i.e., within 3 to 5%) the sampling protocol will become the crux of any validation campaign. Our results have shown that local absorption estimates gathered from canopy volumes containing lots of foliage (i.e., tree crowns) tend to lie above the domain average, whereas those acquired from canopy volumes with little foliage (i.e., gaps in between the tree crowns) tend to lie below. In other words, the spatial distribution of the local sampling points is critical especially if highly accurate estimates of domain-averaged canopy properties are expected. To achieve that goal, efforts will have to be directed towards the design of sampling protocols that account not only for the height and internal variability of a canopy target but also for the illumination conditions at the time of measurement.

Appendix A. Horizontal fluxes and the local energy balance

Consider a coniferous forest uniformly covering a horizontally infinite expanse of flat terrain, and having a tree height probability density function (PDF) that is bounded by some upper limit z^{T}. In choosing this maximum tree height as the reference height for top-of-canopy (TOC) reflectance measurements throughout the entire domain of the forest guarantees that 1) the incident direct and diffuse solar radiation components are the sole contributors toward the TOC boundary condition irrespective of the spatial resolution of observation, and 2) the spatial averages of albedo and bidirectional reflectance factor (BRF) observations over some forested area will remain independent of the spatial resolution S with which that region is observed. Furthermore, by sub-dividing the horizontal expanse of the canopy volume below z^{T} into a regular grid of box-like entities (of height z^{T} and horizontal dimensions $S_{\parallel}=S_{\perp}=S$), whose lateral sides are either parallel ($\parallel$) or perpendicular ($\perp$) to the azimuth direction of the incident direct solar radiation (ϕ_0), allows to study the properties of horizontal photon exchanges and the impact that geometric shading may have at any instant in time and across multiple spatial resolutions within the domain of interest.

The monochromatic intensity $I_\lambda(\mathbf{p},\mathbf{\Omega})$ that passes in or out of the canopy voxel $V(S, z^{\mathrm{T}}; \mathbf{r})$ via some point $\mathbf{p}$ on one of its lateral sides – having an outward normal $\mathbf{n}$ and a surface area A – depends both on the wavelength λ and the direction of travel $\mathbf{\Omega}$. In general, $I_\lambda(\mathbf{p},\mathbf{\Omega})$ includes a direct solar contribution, a diffuse solar contribution, and a contribution due to a previous scattering event in canopy regions outside or inside $V(S, z^{\mathrm{T}}; \mathbf{r})$. Integrating $I_\lambda(\mathbf{p},\mathbf{\Omega})$ over all hemispherical directions (2π) will yield the incoming ($\mathbf{n}\cdot\mathbf{\Omega}<0$) or outgoing ($\mathbf{n}\cdot\mathbf{\Omega}>0$) flux density $\mathrm{F}_{\lambda,p}$[W m^{-2}] at point $\mathbf{p}$ (Lenoble, 1985):

$$\mathrm{F}_{\lambda,p} = \int_{2\pi} |\mathbf{n}\cdot\mathbf{\Omega}| I_\lambda(\mathbf{p},\mathbf{\Omega}) \mathrm{d}\mathbf{\Omega}$$

where the hemisphere is defined around the surface normal $\mathbf{n}$ of the voxel side, and $\mathrm{d}\mathbf{\Omega}=\sin\theta \mathrm{d}\theta \mathrm{d}\phi$. Further integration over all locations $\mathbf{p}$ contained within the corresponding voxel-side A then yields the total flux (or power) F [W m^{-2} m^{-2}] entering or exiting the voxel through that side:

$$F_{\lambda,\mathrm{A}} = \int_{p\in\mathrm{A}} \mathrm{F}_{\lambda,p} \mathrm{d}\mathbf{p} = \mathrm{A}\,\overline{\mathrm{F}}_{\lambda,\mathrm{A}} \tag{1}$$

where $\overline{\mathrm{F}}_{\lambda,\mathrm{A}}=F_{\lambda,\mathrm{A}}/\mathrm{A}$ is the average flux density along the voxel side of interest.

Omitting the wavelength dependency, the total net flux in and out of a voxel centered at some location $\mathbf{r}$, i.e., $\Delta F(S, z^{\mathrm{T}}; \mathbf{r})$ can be decomposed, by analogy to the developments of Titov (1999) and Marshak and Davis (2005), into a contribution due to the horizontally integrated net fluxes across the top and bottom surfaces ($\mathrm{A}^{\mathrm{T}}=\mathrm{A}^{\mathrm{B}}=S\times S$) of the voxel, i.e., $\Delta F_v^{\uparrow\downarrow}$, and another due to the vertically-integrated net photon flow across the four lateral sides ($\mathrm{A}^{\mathrm{L}}=S\times z^{\mathrm{T}}$) of the voxel, i.e., $\Delta F_h^{\rightleftharpoons}$:

$$\Delta F(S, z^{\mathrm{T}}; \mathbf{r}) = \Delta F_v(S; z^{\mathrm{T}}, \mathbf{r}) + \Delta F_h(S, z^{\mathrm{T}}; \mathbf{r}) \tag{2}$$

Using the convention to add (subtract) all incoming (outgoing) energy, one can expand $\Delta F_v^{\uparrow\downarrow}(S, z^{\mathrm{T}}; \mathbf{r})$ as a linear combination of four hemispherical flux contributions entering (in) and exiting (out) the voxel through the top ($\hat{z}=z^{\mathrm{T}}$) and bottom ($\check{z}=0$) surfaces:

$$\Delta F_v(S; \mathbf{r}) = F_{\hat{z}}^{\mathrm{in}}(S; \mathbf{r}) - F_{\hat{z}}^{\mathrm{out}}(S; \mathbf{r}) + F_{\check{z}}^{\mathrm{in}}(S; \mathbf{r}) - F_{\check{z}}^{\mathrm{out}}(S; \mathbf{r}) \tag{3}$$

where the symbols $\hat{}$ and $\check{}$ refer to the maximum and minimum values, respectively, of the coordinate that is kept constant for all points $\mathbf{p}$ belonging to the bounding surface of interest (here coordinate z and surfaces A^{T} and A^{B}). Inserting Eq. (3) within Eq. (2), normalizing both sides by the total incident flux at the top-of-canopy ($F_{\hat{z}}^{\mathrm{in}}$), and re-arranging the various terms will yield the local energy balance of the canopy volume $V(S, z^{\mathrm{T}}; \mathbf{r})$ centered at location $\mathbf{r}$:

$$1 = [A(S, z^{\mathrm{T}}; \mathbf{r}) + R(S, z^{\mathrm{T}}; \mathbf{r}) + (1-\alpha)T(S, z^{\mathrm{T}}; \mathbf{r})] - H(S, z^{\mathrm{T}}; \mathbf{r}) \tag{4}$$

where $A=\Delta F/F_{\hat{z}}^{\mathrm{in}}$ is the absorption within $V(S, z^{\mathrm{T}})$, $R=F_{\hat{z}}^{\mathrm{out}}/F_{\hat{z}}^{\mathrm{in}}$ is the local surface albedo at the TOC boundary A^{T}, $T=F_{\check{z}}^{\mathrm{out}}/F_{\hat{z}}^{\mathrm{in}}$ is the local transmission, and α is the background albedo. $H=\Delta F_h^{\rightleftharpoons}/F_{\hat{z}}^{\mathrm{in}}$ is the horizontal flux describing the ratio of the net horizontal flux densities (vertically-integrated over all lateral sides) and the total incoming flux at the top-of-canopy level, z^{T} (Marshak & Davis, 2005). Given the difference in surface area between the lateral and top-of-canopy voxel sides, i.e., $\mathrm{A}^{\mathrm{L}}(S)/\mathrm{A}^{\mathrm{T}}(S)=z^{\mathrm{T}}/S$, the magnitude of $H(S, z^{\mathrm{T}}; \mathbf{r})\to 0$ as $S\to\infty$ even for voxels that are

completely filled with perfectly absorbing scatterers. As such Eq. (4) becomes:

$$1 = A(S^{\infty}) + R(S^{\infty}) + (1-\alpha)T(S^{\infty}) \quad (5)$$

In the context of vegetation canopies, $H(S, z^{\mathrm{T}}; \mathbf{r})$ thus appears as an error term in Eq. (5), affecting the inherent quantities of A, R and T all together. The manner in which this energy (loss or gain) will be spatially distributed, however, depends on the structural and spectral properties of the 3-D canopy within $V(S, z^{\mathrm{T}})$, but also on the illumination conditions and the canopy structure outside of $V(S, z^{\mathrm{T}})$, since the latter will affect the vertical distribution of the incident (and exiting) lateral radiation into (from) $V(S, z^{\mathrm{T}})$.

Appendix B. The impact of geometric shading on H

The impact of the direct solar radiation contribution on the magnitude of H can be assessed quite conveniently by aligning a voxel such that two of its lateral sides are parallel to the incoming solar azimuth direction ϕ_0. One can thus define $H_{\perp}=H^0_{\perp}+H^d_{\perp}$ as being due to the direct ($H^0_{\perp}$) and diffuse ($H^d_{\perp}$) photon transport across the lateral voxel sides that are perpendicular to the solar azimuth, and $H_{\parallel}=H^d_{\parallel}$ as being due to the diffuse photon flow across those lateral voxel sides that are parallel to the azimuth direction of the incident solar radiation:

$$H(S, z^{\mathrm{T}}; \mathbf{r}) = H_{\perp}(S, z^{\mathrm{T}}; \mathbf{r}) + H_{\parallel}(S, z^{\mathrm{T}}; \mathbf{r})$$

At coarse spatial resolutions, i.e., for $S>S^*$, the diffuse contributions to the net horizontal flux term will be equal $H^d_{\perp}=H^d_{\parallel}$.

Fig. 9 displays the spatial resolution dependent maxima ($\hat{H}$) and minima ($\check{H}$) of the net horizontal flux components across voxel sides that are perpendicular, $H_{\perp}$ (left panel) and parallel, $H_{\parallel}$ (right panel) to the solar azimuth direction. Results are shown for a 300 stem/ha Scots pine forest under different direct illumination conditions in the red spectral domain. Positive (negative) values indicate that more (less) photons enter the voxel through the corresponding lateral sides than exit through the same sides. The difference being due to photons that are absorbed, leave or enter the voxel through other sides. Three major points have to be noticed here: 1) the magnitude of the various net horizontal flux term extremes increases dramatically as the spatial resolution becomes finer, 2) the net horizontal flux terms exhibit an increasing asymmetry in between $\hat{H}$ and $|\check{H}|$ as $S\rightarrow 1$ m, and 3) the magnitude of the $H_{\perp}$ component tends to exceed that of $H_{\parallel}$ at all spatial resolutions.

The primary reason for the increasing magnitudes of $\hat{H}$ and $|\check{H}|$ as $S\rightarrow 1$ m are the changing areas of the top and lateral voxel sides, leading to different (incoming and outgoing) flux contributions even though the canopy structure inside the voxels may not change statistically. In addition, the likelihood that the sunward (lateral) voxel side is either completely illuminated or else entirely shadowed also increases at very high spatial resolutions. The increasing asymmetry between $\hat{H}_{\perp}$ and $|\check{H}_{\perp}|$ as $S\rightarrow 1$ m, on the other hand, is governed by the different amounts of direct solar radiation that enter or exit these voxels, respectively. Consider, for example, the ideal case of a voxel that is completely "filled" with some perfectly absorbing material and surrounded by a large number of "empty" voxels located above a black background. Here the total incident flux at the top of the voxel, $F_{\mathrm{A}^{\mathrm{T}}} = \overline{\mathrm{F}}_0 S^2$, whereas, that intercepted by the sunward lateral side, $F_{\mathrm{A}^{\mathrm{L}}} = \overline{\mathrm{F}}_0 z^{\mathrm{T}} S \tan\theta_0$ where $\overline{\mathrm{F}}_0$ is the mean flux density at the top of the canopy. Since all of the laterally impinging radiation contributes toward a positive net horizontal flux term, and no radiation may exit the "filled" voxel laterally, it will thus give rise to $\hat{H}_{\perp}$ which is equal to $F_{\mathrm{A}^{\mathrm{L}}}/F_{\mathrm{A}^{\mathrm{T}}} = \tan\theta_0 z^{\mathrm{T}}/S$. The "empty" neighbouring voxel that is in the shadow of the above filled voxel, on the other hand, does not receive any lateral inflow of direct solar radiation. Here it is only the incident radiation at the top of the voxel that traverses the voxel and exits laterally, thus giving rise to $\check{H}_{\perp}$ which for $\theta_0 \geq \arctan(S/z^{\mathrm{T}})$ amounts to $F_{\mathrm{A}^{\mathrm{L}}}/F_{\mathrm{A}^{\mathrm{T}}} = -F_{\mathrm{A}^{\mathrm{T}}}/F_{\mathrm{A}^{\mathrm{T}}} = -1$.

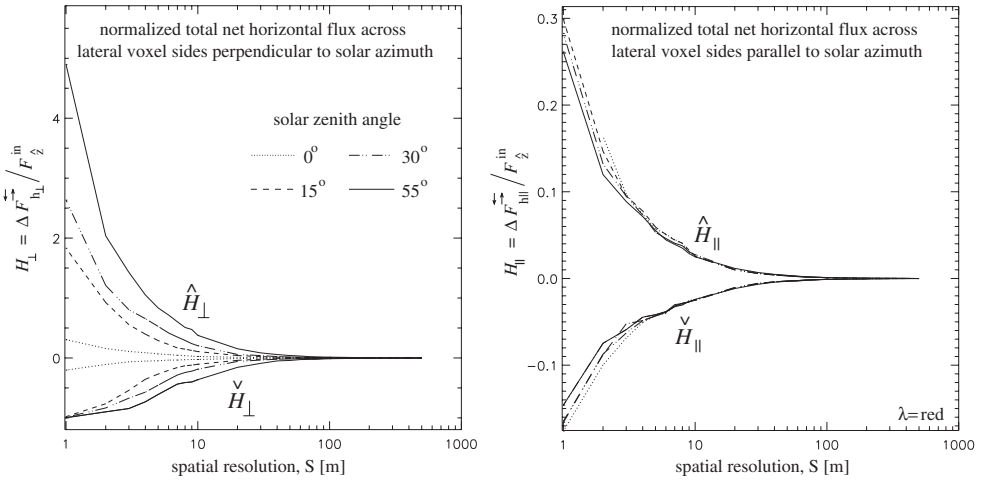

Fig. 9. The maximum (positive values) and minimum (negative values) normalized net horizontal fluxes – across those lateral sides of a voxel that are perpendicular, $H_{\perp}$ (left panel) and parallel, $H_{\parallel}$ (right panel) to the solar illumination azimuth – plotted against spatial resolution. Results are shown in the red spectral band, for different solar zenith angles and a 3-D Scots pine forest with 300 stem/ha.

Hence in the above example the differences between $\hat{H}_\perp$ and $|\check{H}_\perp|$ are likely to widen if the spatial resolution becomes finer, the canopy gets taller, and/or the solar zenith angle increases. This behaviour can indeed be observed in the left hand panel of Fig. 9 despite the fact that for a 300 stem/ha Scots pine forest scene the voxels will never be completely filled nor will the spectral properties of the background and foliage elements ever be equal to zero. Tests (not depicted) have shown that, when plotting the $\hat{H}_\perp(S)$ for this 3-D forest scene against S on a log–log plot, the decrease in $\hat{H}_\perp(S \geq z^{\mathrm{T}} \tan\theta_0)$ is not proportional to S^{-1} as prescribed by the black canopy and background example above ($\hat{H}_\perp = \tan\theta_0 z^{\mathrm{T}}/S$), but rather faster, i.e., $H_\perp \propto S^{-1.6}$. It was also noted that the onset of this power law behaviour occurred around $S \approx z^{\mathrm{T}} \tan\theta_0$, with the magnitude of the exponent getting smaller as the stem density increases, whilst being relatively insensitive to changes in illumination conditions or wavelength. At this stage it is not exactly clear what the reasons for this faster decrease may be, but we conjecture that it is related to the number and sizes of canopy gaps, as well as the multiple-scattering interactions within the canopy that tend to reduce the net horizontal radiation imbalance of a voxel. Finally, it is also interesting to note that, in the right hand panel of Fig. 9, the maximum $|\hat{H}_{||}|$ and minimum $|\check{H}_{||}|$ net horizontal flux terms – arising only from radiation that has been scattered laterally by the canopy – are increasingly different as the spatial resolution becomes finer. Given that all canopy constituents, including the background, obey Lambertian scattering laws this asymmetry can be explained purely on the grounds of the finite size of the voxels: The amount of radiation that is scattered from a spatially infinite lambertian background laterally into a completely filled and perfectly absorbing voxel (maximum positive contribution to H^d) will always be larger than the amount of radiation that exits from an empty voxel into its – completely filled and perfectly absorbing – surroundings (maximum negative contribution to H^d). As a consequence the differences between $\hat{H}_{||}$ and $|\check{H}_{||}|$ will decrease as the size of the voxel gets larger.

By comparing the two panels of Fig. 9 one notices that the magnitude of $|H_\perp|$ exceeds that of $|H_{||}|$ at all spatial resolutions due to the direct illumination component $H^0_\perp$ if $\theta_0 > 0°$. Indeed, for overhead illumination conditions, $H_\perp$ does not contain any direct illumination component, i.e., $H_\perp = H^d_\perp \approx H^d_{||}$. Since only those photons contribute toward $H^d_{||}$ and $H^d_\perp$ that have experienced at least one interaction with either background or canopy attributes – all of which having non-conservative scattering properties in the red – the direct component $H^0_\perp$ is always going to be larger than $H^d_\perp$ (or $H^d_{||}$) even at very coarse spatial resolutions. As the solar zenith angle increases so do the ratii between $|\hat{H}_\perp|/|\hat{H}_{||}|$ and $|\check{H}_\perp|/|\check{H}_{||}|$. This is a clear indication that, at least at the higher spatial resolutions, geometric shading dominates the extremes of the net horizontal radiation transport in the red wavelength regime, since the total incident flux, $F^{\mathrm{in}}_{\hat{z}}$ at the top of any given voxel was kept independent of θ_0. In fact it was found that even at the coarser spatial resolutions in the red spectral regime the total net horizontal flux term, H is highly dominated by the magnitude of $H_\perp$ provided that the canopy volume is not too densely packed and the background is of average brightness. This agrees well with the findings of Várnai (2000), who investigated cloud-top-height variations under oblique illumination conditions, and noted the dominant impact that geometric shading may have on the measured brightness value of a pixel.

References

Cahalan, R., Ridgeway, W., Wiscombe, W. J., & Bell, T. (1994). The albedo of fractal stratocumulus clouds. *Journal of the Atmospheric Sciences*, *51*, 2434–2455.

Chen, J. M., Blanken, P. D., Black, T. A., Guilbeault, M., & Chen, S. (1997). Radiation regime and canopy architecture in a boreal Aspen forest. *Agricultural and Forest Meteorology*, *86*, 107–125.

Chen, J. M., & Cihlar, J. (1995). Plant canopy gap size analysis theory for improving optical measurements of leaf area index. *Applied Optics*, *34*, 6211–6222.

Davis, A. B., Marshak, A., Wiscombe, W. J., & Cahalan, R. F. (1996). Scale invariance in liquid water distributions in marine stratocumulus. Part I: Spectral properties and stationarity issues. *Journal of the Atmospheric Sciences*, *53*, 1538–1558.

Diner, D. J., Braswell, B. H., Davies, R., Gobron, N., Hu, J., Jin, Y., et al. (2005). The value of multiangle measurements for retrieving structurally and radiatively consistent properties of clouds, aerosols and surfaces. *Remote Sensing of Environment*, *97*, 495–518.

Franklin, J., Michaelsen, J., & Strahler, A. H. (1985). Spatial analysis of density pattern in coniferous forest stands. *Vegetatio*, *64*, 29–36.

Gobron, N., Pinty, B., Aussedat, O., Chen, J. M., Cohen, W. B., Fensholt, R., et al. (in press). Evaluation of FAPAR products for different canopy radiation transfer regimes: Methodology and results using JRC products derived from SeaWiFS against ground-based estimations. *Journal of Geophysical Research*.

Gobron, N., Pinty, B., Verstraete, M. M., & Govaerts, Y. (1999). The MERIS Global Vegetation Index (MGVI): description and preliminary application. *International Journal of Remote Sensing*, *20*, 1917–1927.

Govaerts, Y., & Verstraete, M. M. (1998). Raytran: a Monte Carlo ray tracing model to compute light scattering in three-dimensional heterogeneous media. *IEEE Transactions on Geoscience and Remote Sensing*, *36*, 493–505.

Huemmrich, K. F., Privette, J. L., Mukelabai, M., Myneni, R. B., & Knyazikhin, Y. (2005). Time-series validation of MODIS land biophysical products in a Kalahari woodland, Africa. *International Journal of Remote Sensing*, *26*, 4381–4398.

Kint, V. (2005). Structural development in ageing temperate Scots pine stands. *Forest Ecology and Management*, *214*, 231–250.

Knyazikhin, Y., Martonchik, J. V., Diner, D. J., Myneni, R. B., Verstraete, M. M., Pinty, B., et al. (1998). Estimation of vegetation canopy leaf area index and fraction of absorbed photosynthetically active radiation from atmosphere-corrected MISR data. *Journal of Geophysical Research*, *103*, 32,239–32,256.

Lenoble, J. (1985). *Radiative transfer in scattering and absorbing atmospheres: Standard computational procedures.* Hampton, VA, USA: A. Deepak Publishing.

Lepš, J., & Kindlmann, P. (1987). Models of the development of spatial pattern of an even-aged plant population over time. *Ecological Modelling*, *39*, 45–57.

Marshak, A. L., & Davis, A. B. (2005). Horizontal fluxes and radiative smoothing. In A. B. Davis, & A. L. Marshak (Eds.), *Three-dimensional radiative transfer in the cloudy atmosphere* New York: Springer-Verlag ISBN 10 (3-540-23958-8).

Marshak, A. L., Davis, A. B., Wiscombe, W. J., & Cahalan, R. F. (1995). Radiative smoothing in fractal clouds. *Journal of Geophysical Research*, *100*, 26,247–26,261.

Mélin, F., Steinich, C., Gobron, N., Pinty, B., & Verstraete, M. M. (2001). Optimal merging of LAC and GAC data from SeaWiFS. *International Journal of Remote Sensing*, *23*, 801–807.

Moeur, M. (1993). Characterizing spatial patterns of trees using stem-mapped data. *Forest Science*, *39*, 756–775.

Morisette, J. T., Baret, F., Privette, J. L., Myneni, R. B., Nickeson, J., Garrigue, S., et al. (in press). Validation of global moderat resolution LAI products: A framework proposed within the CEOS Land Product Validation subgroup. *IEEE Transactions on Geoscience and Remote Sensing*.

Pinty, B., Gobron, N., Widlowski, J. -L., Lavergne, T., & Verstraete, M. M. (2004). Synergy between 1-D and 3-D radiation transfer models to retrieve vegetation canopy properties from remote sensing data. *Journal of Geophysical Research*, *109*, doi:10.1029/2004JD005214, D21205.

Rautiainen, M., & Stenberg, P. (2005). Simplified tree crown model using standard forest mensuration data for Scots pine. *Agricultural and Forest Meteorology*, *128*, 123–129.

Schaaf, C. B., Gao, F., Strahler, A. H., Lucht, W., Li, X., Tsang, T., et al. (2002). First operational BRDF, albedo and nadir reflectance products from MODIS. *Remote Sensing of Environment*, *83*, 135–148.

Schuster, A. (1905). Radiation through a foggy atmosphere. *Astrophysical Journal*, *21*, 1–22.

Szczap, F., Isaka, H., Saute, M., Guillemet, B., & Ioltukhovski, A. (2000). Effective radiative properties of bounded cascade absorbing clouds: Definition of an effective single-scattering albedo. *Journal of Geophysical Research*, *105*, 20635–20648.

Szwagrzyk, J. (1992). Small-scale spatial patterns of trees in a mixed *Pinus sylvestris–Fagus sylvatica* forest. *Forest Ecology and Management*, *51*, 301–315.

Tian, Y., Wang, Y., Zhang, Y., Knyazikhin, Y., Bogaert, J., & Myneni, R. B. (2002). Radiative transfer based scaling of LAI retrievals from reflectance data of different resolutions. *Remote Sensing of Environment*, *84*, 143–159.

Titov, G. (1990). Statistical description of radiation transfer in clouds. *Journal of the Atmospheric Sciences*, *47*, 24–38.

Titov, G. (1998). Radiative horizontal transport and absorption in stratocumulus clouds. *Journal of the Atmospheric Sciences*, *55*, 2549–2560.

Turner, D. P., Ritts, W. D., Cohen, W. B., Maeirsperger, T., Gower, S. T., Kirschbaum, A., et al. (2004). Site-level evaluation of satellite-based global terrestrial GPP and NPP modeling. *Global Change Biology*, *11*, 666–684.

Várnai, T. (2000). Influence of three-dimensional radiative effects on the spatial distribution of shortwave cloud reflection. *Journal of the Atmospheric Sciences*, *57*, 216–229.

Wang, Y., Woodcock, C. E., Buermann, W., Stenberg, P., Voipio, P., Smolander, H., et al. (2004). Evaluation of the MODIS LAI algorithm at a coniferous forest site in Finland. *Remote Sensing of Environment*, *91*, 114–127.

Widlowski, J. -L., Pinty, B., Gobron, N., & Verstraete, M. M. (2003). Allometric relationships of selected European tree species. *Technical report EUR 20855 EN.* Ispra, Italy: EC Joint Research Centre.

Widlowski, J. -L., Pinty, B., Gobron, N., Verstraete, M. M., Diner, D. J., & Davis, A. B. (2004). Canopy structure parameters derived from multi-angular remote sensing data for terrestrial carbon studies. *Climatic Change*, *67*, 403–415.

Wu, Y., & Strahler, A. H. (1994). Remote estimate of crown size, stand density and biomass on the Oregon transect. *Ecological Applications*, *4*, 299–312.